# Spectroscopic and structural characteristics of a dual-light sensor protein, PYP-phytochrome related protein

**SUM JIA SIANG**

**Graduate School of Materials Science**

**Nara Institute of Science and Technology**

2020

**ABSTRACT**

PYP-phytochrome related (Ppr) protein absorbs both blue and red light by photoactive yellow protein (PYP) and bacteriophytochrome (Bph) light sensor domains, which contains *p*-coumaric acid (pCA) and biliverdin (BV) as chromophores, respectively. While the dual-light sensor setup enables Ppr responds to light signals with different wavelength, the role of the dual –light sensor system is still unknown. In order to understand it, this thesis focuses on the interdependency of the photoreactions of PYP and Bph. I performed spectroscopic and structural analyses of Ppr under dark and various light irradiation conditions.

This thesis is divided into two experimental chapters. The first chapter describes the spectroscopic characterization of the Ppr photoreactions under red and/or blue light irradiation. I prepared three variants of Ppr, which are the intact Ppr containing both of the chromophores, Holo-Holo-Ppr (H-H-Ppr), H-A-Ppr lacking BV, and A-H-Ppr lacking pCA. UV-Vis absorption spectra of H-H-Ppr under the dark and the light conditions reveal that the red light triggers the photoreaction only in Bph, but the blue light simultaneously excites both PYP and Bph. However, within the first 250 seconds of blue light irradiation, significant spectrum changes can be observed in the wavelength between 300 and 500 nm, which can be attributed to the photoreaction in PYP. Carefully comparing the difference spectra in different time domains within the 250 sec, there is a slight but detectable difference. While the beginning stage shows two broad positive peaks, the latter stage only displays one prominent peak at the $\lambda_{max}$ of 350 nm. This spectrum change can be understood by assuming the transition from $PYP_L$ to $PYP_M$ intermediates. Furthermore, upon the formation of $PYP_M$, the spectrum of Bph also shows slight red-shift, indicating that $PYP_M$ influences the chromophore environment of Bph. From these facts, it can be postulated that Ppr accompanied by $PYP_M$ undergoes structural change in the spatial arrangement of PYP and Bph, resulting in the alteration of the chromophore environment

of Bph.

The second chapter focuses on the structural characteristics of Ppr to confirm the hypothesis of the structural change triggered by the photoreaction of PYP. Firstly, to investigate the spatial relation between PYP and Bph, ab initio molecular envelope modeling of the dark state Ppr was carried out by using SAXS measurements. The Guinier analysis shows that Ppr takes a dimeric form. The envelope offers an arrangement of each domain in the whole molecule. The resulting low-resolution structure envelope is manually superposed with X-ray crystallographic structures of individual homologous domains reported so far. The model demonstrates close proximity of PYP and Bph with each other, indicating that the photoreactions of PYP and Bph can be possibly coupled with each other through the spatial interface. The SAXS profiles at the dark and the blue light irradiation shows substantial difference around 0.05 $Å^{-1}$, indicating the presence of structural rearrangement in Ppr. Time-resolved SAXS measurements were also performed. The intensity around 0.05 $Å^{-1}$ increases up to 250 sec starting from the continuous blue light irradiation and subsequently decreases after 250 sec irradiation. In the time domain after 250 sec, the photoproduct of Bph (Bph*) is accumulated, and the amount of $PYP_M$ concomitantly decreases. From these results, it can be proposed that the formation of $PYP_M$ triggers structural change in Ppr, then the structural change is suppressed due to the subsequent formation of Bph*.

The low-resolution modeling of Ppr reveals the proximity of PYP and Bph. The UV-Vis measurements indicate that the photoreactions of PYP and Bph are tightly coupled to each other. It should be emphasized that Ppr containing $PYP_M$ undergoes large structural change, and the activation of Bph suppresses the structural change. In other words, the structural change triggered by the blue light is suppressed by the red light or the continuous long-term blue light

irradiation through the alteration of the reaction characteristics of PYP coupled with the reaction of Bph. The functionally active form of Ppr is still unknown. However, assuming the observed structural change can mediate the binding affinity of interaction partners, the dual-light sensor system of Ppr can be proposed to realize the On/Off regulation depending on various environmental light conditions such as different intensity, colors, irradiation duration, and so on.

**LIST OF ABBREVIATIONS**

| | |
|---|---|
| Bph | bacteriophytochrome domain |
| $Bph_D$ | dark state Bph |
| Bph* | photoactivated Bph |
| BV | biliverdin |
| CheW | chemotaxis protein CheW |
| chsA | chalcone synthase A |
| Cph | cyanobacterial phytochrome |
| Da | dalton |
| *Dr*BphP | bacteriophytochrome of *Deinococcus radiodurans* |
| DTT | dithiothreitol |
| EDTA | ethylenediaminetetraacetic acid |
| Fph | fungal phytochrome |
| GAF | cGMP-specific phosphodiesterase/adenylate cyclases/FhlA |
| *Hh*-PYP | PYP of *Halorhodospira halophila* |
| HK | histidine kinase |
| I(0) | zero scattering angle |
| LED | light emitting diode |
| $P_{fr}$ | far-red light absorbing |
| $P_{nr}$ | near-red light absorbing |
| $P_o$ | orange light absorbing |
| $P_r$ | red light absorbing |
| P(r) | pair-distance distribution function |
| PAS | Per/ARNT/Sim |
| pCA | *p*-coumaric acid |

| | |
|---|---|
| PDB | protein data bank |
| Ppr | PYP-phytochrome related |
| H-H-Ppr | Holo-Holo-Ppr |
| H-A-Ppr | Holo-Apo-Ppr |
| A-H-Ppr | Apo-Holo-Ppr |
| Ppr-PYP | Truncated Ppr with only PYP domain |
| PHY | phytochrome-specific |
| PYP | photoactive yellow protein domain |
| $PYP_D$ | dark state PYP |
| PYP* | photoactivated PYP |
| $PYP_L$ | $PYP_L$-like |
| $PYP_M$ | $PYP_M$-like |
| $R_g$ | radius of gyration |
| SAXS | small angle X-ray scattering |
| SEC | size exclusion chromatography |

List of program abbreviations under ATSAS software without definite full terms:

CRYSOL

DAMAVER

DAMCLUST

DAMMIN

DAMSTART

PRIMUS

**CONTENTS**

## CHAPTER 1: General Introduction

Living organisms respond to various environmental factors and external stimulation to survive. These factors could be chemical gradient, temperature difference and light intensity. Depending on the nature of the stimulation, the response encompasses relocation to favorable nutrient sources or escape from harm's way. At least three billion years ago, early living organisms utilize light sensing proteins to aid in locating sunlight. Since then, various light sensing proteins have evolved to fulfill different biological functions that rely on the detection of light radiation. One such protein is the phytochromes. Phytochromes found in plants are known to absorb red light ($P_r$) in its ground state and switched to far-red light absorbing ($P_{fr}$) state when exposed to red light. These two $P_r$/$P_{fr}$ states are reversible and acts as a photoswitch. In the past, phytochromes were thought to be only found within the plants. The exclusiveness of phytochromes to plants no longer holds true with the advance in genome sequencing which results in the discoveries of other phytochromes species such as cyanobacterial phytochrome (Cph), fungal phytochrome (Fph) and bacteriophytochrome in the late 1990s (1–3).

### 1.1 Bacteriophytochrome

Bacteriophytochrome can be found in both photosynthetic and non-photosynthetic bacteria. Canonical bacteriophytochrome contains PAS (Per/ARNT/Sim), GAF (cGMP-specific phosphodiesterase/adenylate cyclases/FhlA) and PHY (phytochrome-specific) domains at the N-terminal ends which collectively forms the photosensory domain (2, 4–6). The C-terminal end mostly consist of a histidine kinase (HK) which act as the output domain. Together both photosensory and HK domains participate in the phosphorylation regulatory system depending on the light environment. Bacteriophytochrome utilizes biliverdin (BV) as the chromophore (Figure 1-1A) (7) and this is structurally confirmed by studies on *Dr*BphP from *Deinococcus radiodurans* (Figure 1-2), showing BV covalently attached through a thioether linkage with

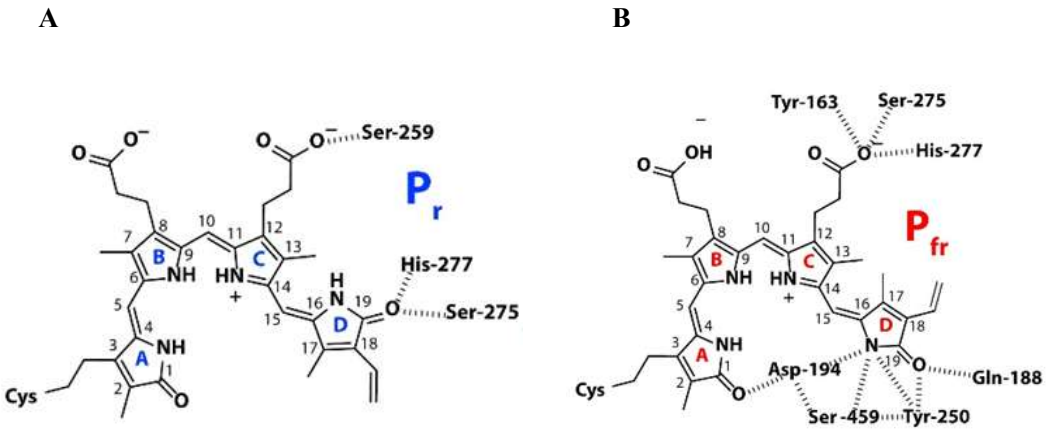


**Figure 1-1.** (A) BV chromophore in $P_r$ state. (B) BV chromophore in $P_{fr}$ state.

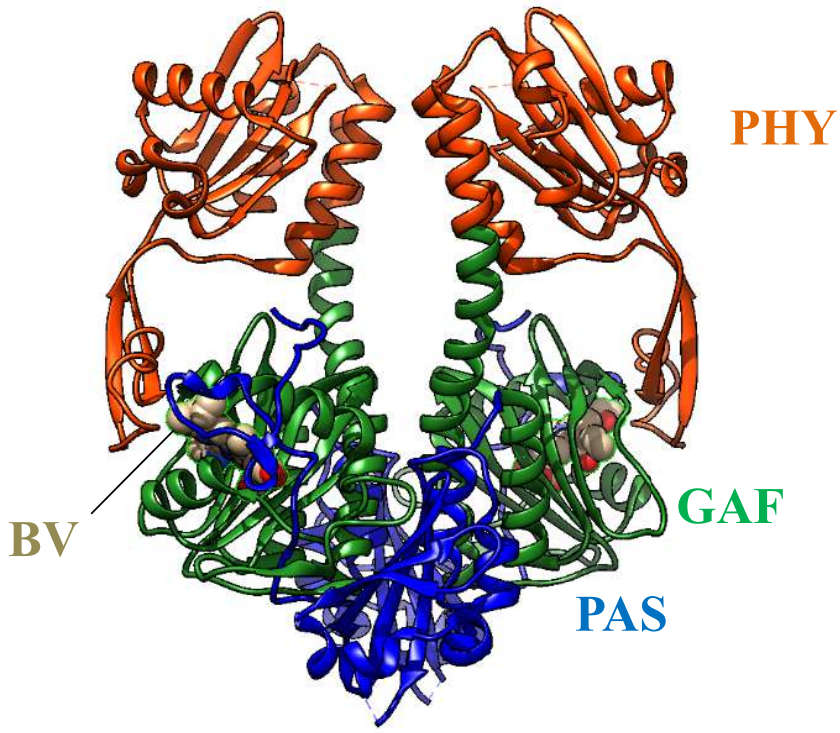


**Figure 1-2.** Bacteriophytochrome of Deinococcus radiodurans (*Dr*BphP), PAS-GAF-PHY configuration. (PDB code 4Q0J) BV molecule embedded within the GAF domain.

cysteine residue in the photosensory domain (8). The BV chromophore is responsible for the red light absorption properties of bacteriophytochrome. Typically, bacteriophytochrome photoconverts between stable $P_r$ and metastable $P_{fr}$ forms. While other bacteriophytochrome such as those from *Bradyrhizobium* and *Rhizobiales* sp. maintain a reverse conversion with $P_{fr}$ being the stable ground state form (9, 10). Some other less common photoreaction states are also known such as the near-red absorbing ($P_{nr}$) form (11) and orange absorbing ($P_o$) form (12). Standing out from the rest, one of the bacteriophytochrome species contains two photosensory domains is known as PYP-phytochrome related (Ppr) protein (Figure 1-3). The bacteriophytochrome Ppr can be found in *Rhodospirillum centenum*. The similar Ppr configuration protein domains could also be found in *Methylobacterium* sp. however not much is known about *Methylobacterium* sp. as of current.

### 1.2 *Rhodospirillum centenum* and Ppr

Based on the earliest published record, *R. centenum* (also known as *Rhodocista centenaria*) was first isolated from samples collected from Thermopolis Hot Springs in Wyoming (13–15). It is a purple nonsulfur bacterium that undergoes aerobic heterotroph growth in the dark. Under exposure of light, it undegoes anaerobic photosynthetic growth. *R. centenum* demonstrates the ability to migrate toward or away from light depending on wavelength of excitation by using its surface-induced flagella, chemotaxis and a photosynthetic apparatus (16, 17). In a study done by Ragatz *et al.* in 1995, *R. centenum* demonstrated phototactic behavior of being attracted to light source longer than 750 nm and repulsive to light source in the 550 nm region. In the following years, mutagenic study of *R. centenum* chemotactic proteins demonstrates a strong relation between chemotactic response and phototactic response (18, 19).

In the year 1999, Ppr protein was discovered in purple photosynthetic bacterium

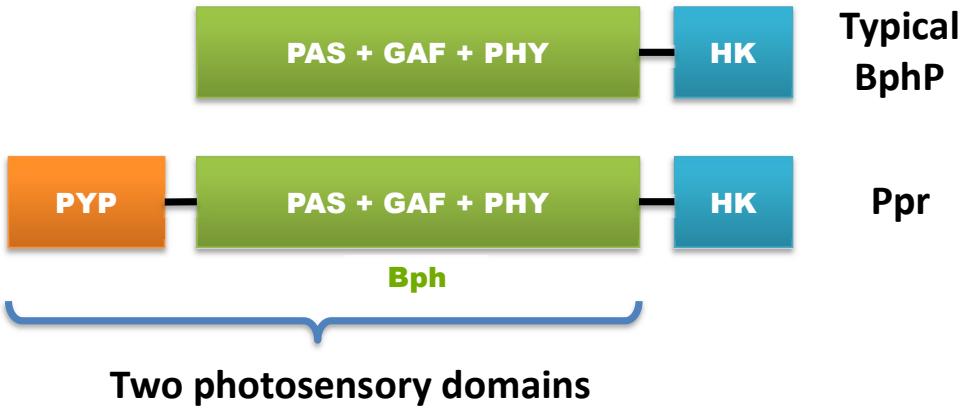


**Figure 1-3.** Full length Ppr consists of PYP domain, Bph domain and HK domain, an extra light sensing domain compared with canonical bacteriophytochrome such as *Dr*BphP. Each PYP domain and Bph domain contains their own chromophore.

*R. centenum* (20) and its genome sequence determined eleven years later (21) (Figure 1-4). Similar to other canonical bacteriophytochrome, Ppr contains of PAS-GAF-PHY photosensory core and a HK output domain. The photosensory core is collectively term as Bph domain in this study. In addition, Ppr has a photoactive yellow protein (PYP) at its N-terminal end (20). In total, the molecular weight of Ppr averaged at 95 kDa.

Setting Ppr apart from other classical bacteriophytochrome, Ppr is able to absorb blue and red light using *p*-coumaric acid (pCA) and BV acting as chromophores respectively. Study suggests that Ppr regulates the expression of chalcone synthase gene (*chsA*) (20) and development of cyst (22), demonstrating highest expression of *chsA* under infrared light. Additional presence of blue light suppress *chsA* expression (20). In addition, HK domain of Ppr is shown to bind with chemotactic protein CheW (23). Together with the information that chemotactic response related to phototactic response, these findings suggest Ppr has a role to play in phototactic response in *R. centenum*.

Despite sharing a similar PAS-GAF-PHY configuration with other bacteriophytochrome species which utilize BV as the chromophore, red light irradiated Ppr demonstrates a decreased Bph absorption spectrum instead of being red-shifted (24) (Figure 1-5). In addition, studies on other bacteriophytochromes such as *Dr*BphP reported bacteriophytochrome is able to toggle its tertiary structure between $P_r$ and $P_{fr}$ states (25, 26). However, until now there is no evidence of Ppr undergoes any such kind of structure change when exposed to red light irradiation.

Regarding the PYP domain, it is homologous to a blue light sensing PYP protein first discovered in *Halorhodospira halophila* (*Hh*-PYP) (27). Over the years, the photocycle model


**Figure 1-4.** Protein sequence of Ppr with three of its domains highlighted.

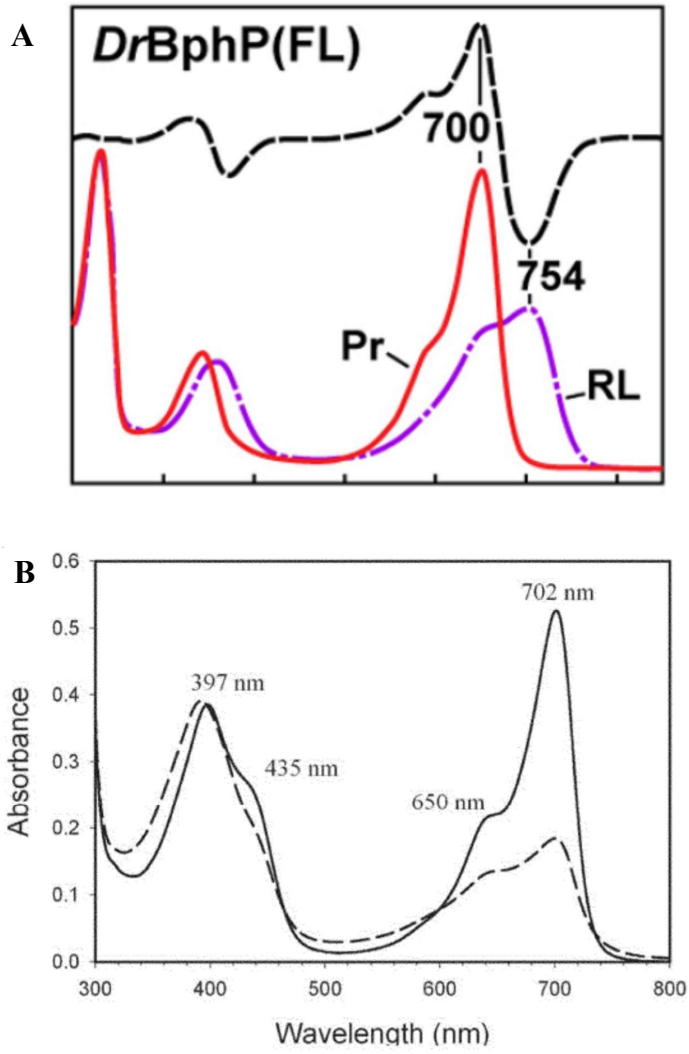


**Figure 1-5.** (A) UV-Visible spectroscopic data of $P_r$ (red line) and $P_{fr}$ (purple line) state of *Dr*BphP. Difference spectrum between $P_r$ ad $P_{fr}$ represented by black line. [Figure adapted from Burgie *et al.*, 2014] (B) UV-Visible spectroscopic data of dark state (solid line) and red light irradiated (dash line) state of Ppr. [Figure adapted from Kyndt *et al.*, 2004]

of *Hh*-PYP is increasingly complex as more studies reveal its underlying mechanisms (28–30). Though, the photocycle could be summarized into 3 states, namely the ground state PYP, the red-shifted intermediate $PYP_L$ and the blue-shifted intermediate $PYP_M$ (31) (Figure 1-6A). Both photointermediates has its own characteristic absorption difference peaks, 470 nm peak for $PYP_L$ and 350 peak for $PYP_M$ (Figure 1-6B). Currently, the transducer protein and biological role for PYP remains largely unknown. However in *R. centenum*, PYP is a part of the genetic coding for Ppr protein together with Bph and HK domains. This genetic setup present a unique opportunity to study the interactions of PYP domain with other protein domains. So, this kind of dual-light sensor setup in Ppr poses a new question, why two sensors are needed as opposed to only one as seen in other phytochrome species? What role does this dual-light setup plays?

As of current gathered knowledge, there are many studies done separately on PYP and Bph based on other bacteria species such as *Halorhodospira halophila* (32), *Deinococcus radiodurans* (7, 25, 26, 33) and *Rhodopseudomonas palustris* (34, 35). These studies gave us the insight to some of the properties that could be related to Ppr considering closely related phytochrome species has well conserved protein structure vital for maintaining its core functionality. For example, *Dr*BphP shows a difference in structural conformation between $P_r$ state under dark and $P_{fr}$ state under red light irradiation. The 2 separate monomers of PHY domains are further apart in $P_{fr}$ state (25, 33) (Figure 1-7). In *Dr*BphP, absence of HK domain from the Bph domain slows down dark recovery to $P_r$ state. In addition, loss of GAF dimerization completely does not dark revert at all (36). However, there is no information on how Bph potentially interacts with PYP protein. Furthermore, the lack of information on the solution structure of full length Ppr protein complex in other Ppr studies limits them from drawing a much deeper comprehension the working mechanisms of Ppr as pointed by Kyndt (37). Gaining this data will potentially give us a better clue on the interaction between PYP and

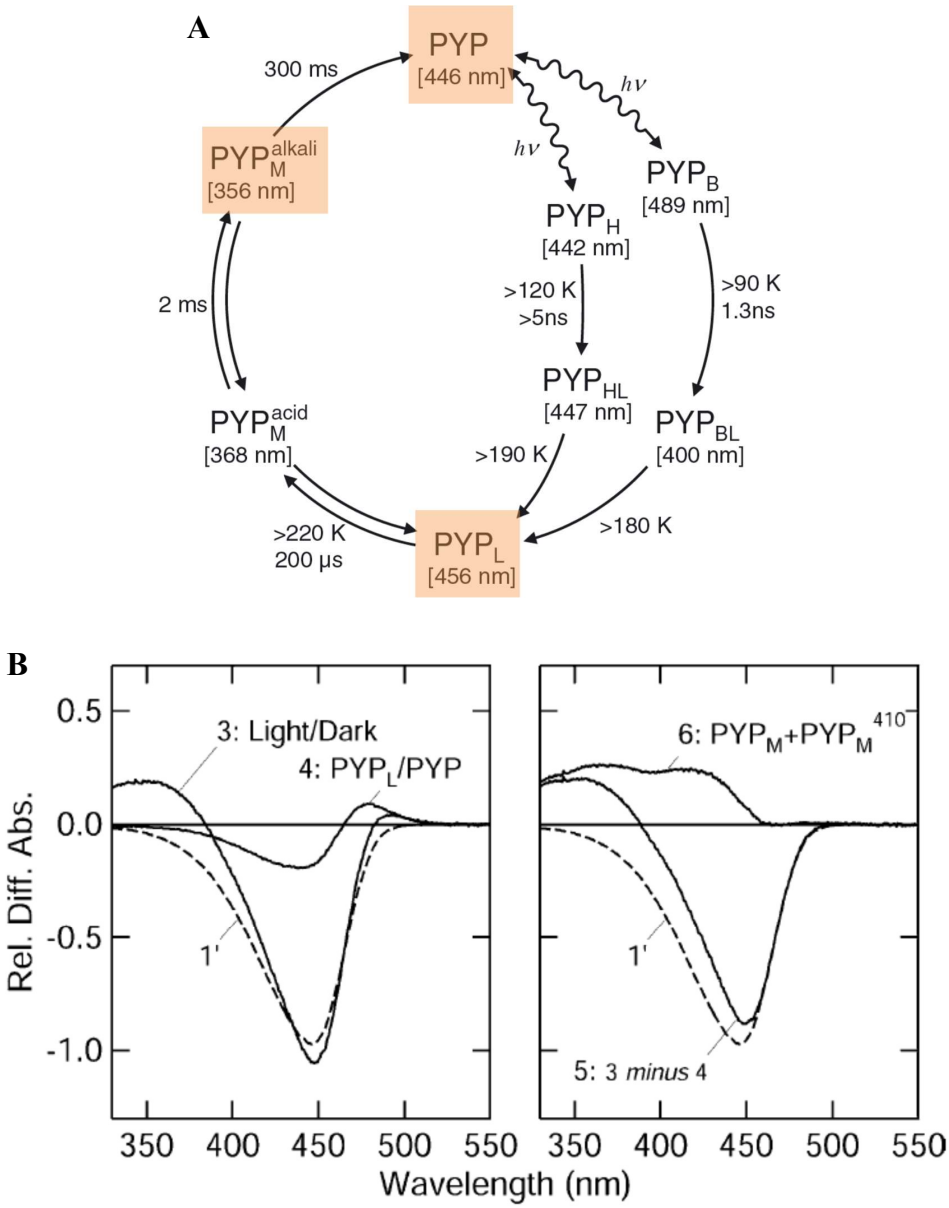


**Figure 1-6.** (A) Photocycle of PYP indicated by steady-state spectroscopy. [Figure adapted from Imamoto & Kataoka, 2007] (38) (B) Curve 4 represent the difference spectrum for $PYP_L$ photospecies against dark state PYP. Curve 5 approximates difference spectrum for $PYP_M$ photospecies against dark state PYP. [Figure adapted from Imamoto *et al.*, 2004]

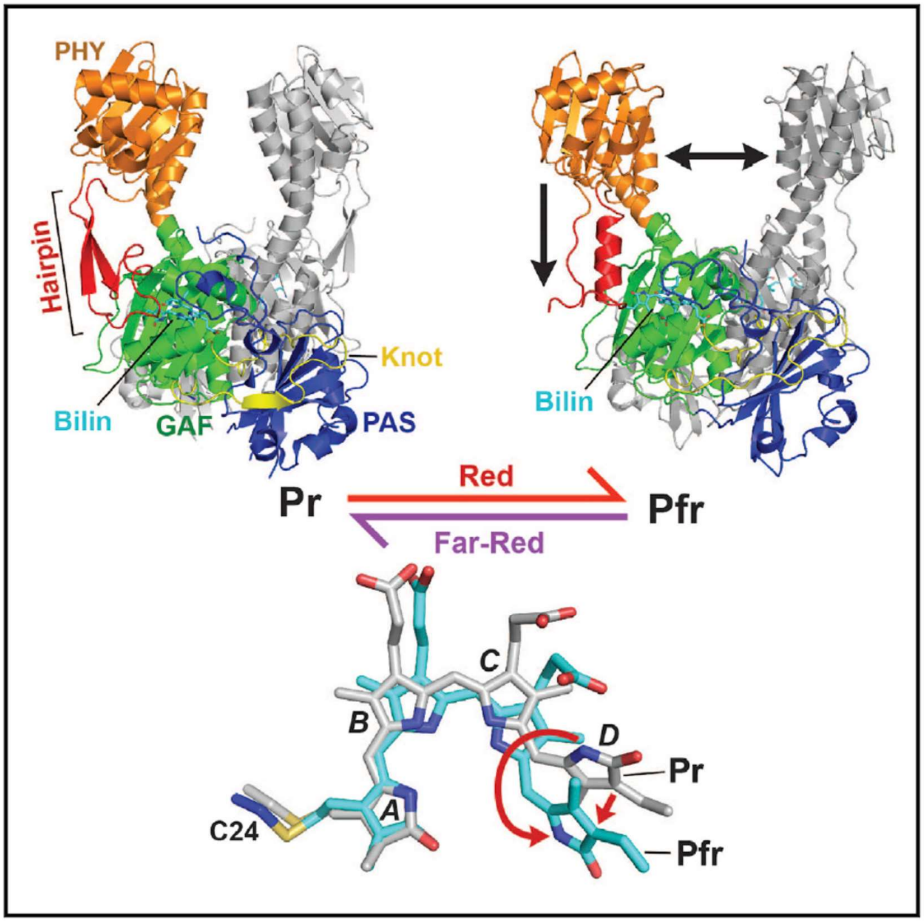


**Figure 1-7.** Structural information of *Dr*BphP in its $P_r$ and $P_{fr}$ states. [Figure adapted from Burgie *et al.*, 2016]

Bph of Ppr which in turn help us understand how HK domain affects downstream reactions.

### 1.3 Purpose of this study

In order to study and elucidate the interactions between PYP and Bph within Ppr, an approach to photoconvert individual chromophores of each protein domain one at a time is needed. Knowing that pCA and BV correspond with PYP domain and Bph domain respectively, Ppr proteins in three different apo and holo forms were prepared: Ppr containing both pCA and BV, Holo-Holo-Ppr (H-H-Ppr); Ppr containing only BV, Apo-Holo-Ppr (A-H-Ppr); and Ppr containing only pCA, Holo-Apo-Ppr (H-A-Ppr). Spectroscopic data was recorded for these variants of Ppr which are subjected to different light irradiation conditions using blue and red light to trigger different parts of the Ppr domains. The idea was to circumvent the issue of overlapping light absorbing region between PYP and Bph chromophores around 400 nm wavelength, allowing the observations of individually photoactivated chromophore and its effect on the associated domain. While changing the chromophore presence, amino acid chain of Ppr remained the same for all Ppr variants to minimize any possible influence to the chromophore environment due to different amino acid sequence.

Unfortunately, there is no structural information available for Ppr to date. As pointed out by Björling (39), spectroscopic measurements has its limitation to only revealing the chromophore's local environment. Coupled with spectroscopic data, an additional structural information of Ppr would provide better understanding to the signaling mechanisms of Ppr. In addition to the spectroscopic measurements, we carried out small angle X-ray scattering (SAXS) measurement on H-H-Ppr under red or blue light irradiation conditions to probe the tertiary structure of Ppr against ground state Ppr. This experiment provide us a valuable information in which condition the Ppr undergoes any large structural changes, which gives us

a clue to the Ppr configuration responsible for its potential signaling state. Here, the author would like to highlight the unusual properties seen in Ppr under blue light irradiation, which PYP plays an active role with Bph in order to bring out conformation change in Ppr.

## CHAPTER 2: UV-Visible Spectroscopic Characterization of Ppr

### 2.1 Background

Given that Ppr is a light sensitive protein, UV-Visible spectroscopic technique can be utilized to probe the light absorption property of the Ppr protein in its different molecular conformation. It is well known that chromophores, molecules capable of light absorption due to its electronic conjugation system, are capable of inducing structural change in protein containing it upon light excitation. This process involves the chromophore changes its molecular structure upon light energy absorption, for example a *trans-cis* isomerization conformation change, which in turn affects its molecular interaction or bonding with surrounding amino acid. This small alteration has the potential to trigger a string of changes that could ultimately distort the protein structure as a whole. As the environment of the chromophore changes, so does its energy state and its light absorption wavelength capabilities. UV-Visible spectroscopic technique able to detect these changes in the chromophore which may help clarify the mechanisms involved behind these changes.

Specifically in this study, the aim is to probe the photoreactions of Ppr chromophores, namely the pCA in PYP domain and BV in Bph domain while subjecting them to different excitation light. These photoreactions would reveal the relative molecular conditions of the chromophore along with its environment pocket, which could potentially translate into alteration experienced by its protein domain host. However, due to the partial overlapping of absorbing wavelength around the blue light region for both pCA and BV in their respective protein domains, a slight modification to Ppr is needed to allow excitation of a single chromophore.

To rectify the issue stated above, Ppr proteins in three different apo and holo forms were

prepared: Ppr containing both pCA and BV, Holo-Holo-Ppr (H-H-Ppr); Ppr containing only BV, Apo-Holo-Ppr (A-H-Ppr); and Ppr containing only pCA, Holo-Apo-Ppr (H-A-Ppr). Spectroscopic data was recorded for these variants of Ppr which are subjected to different light irradiation conditions using blue and red light to trigger different parts of the Ppr domains.

## 2.2 Experiments

### 2.2.1 Protein expression and purification

Double plasmids H-A-Ppr expression system was constructed and transformed into *Escherichia coli* BL21(DE3) as previously reported (40). The *Rhodobacter capsulatus* TAL and pCL genes were in the pACYCDuet1 vector (Novagen) and the Ppr gene of *R. centenum* was in the pET16b vector. Culture was grown in 800 mL LB medium with ampicillin (50 μg/mL) and chloramphenicol (10 μg/mL). At $OD_{600}$ of 0.4 - 0.7, IPTG was added to 1 mM concentration. Induction was carried out at 20 °C, 120 rpm for 16 hours. Cell pellets were resuspended in 50 mM $NaH_2PO_4$, 40 mM NaCl, 2% glycerol and 1 mM DTT (pH 7.4) and disrupted on ice with sonicator (40% duty cycle, 2 minutes for 5 times). Suspension was centrifuged at 30,000 g for 1 hour at 4 °C. Resulting supernatant was proceeded to purification steps for H-A-Ppr preparation. Additional procedure of introducing BV in excess was done for H-H-Ppr preparation. Supernatant was purified through Ni Sepharose™ 6 Fast Flow column (GE Healthcare) in final buffer containing 500 mM imidazole. This is followed by HiLoad 16/60 Superdex 200 pg size exclusion chromatography (SEC) with ÄKTA Explorer in final buffer 25 mM Tris-HCl, 50 mM NaCl, 2% glycerol, 5 mM EDTA and 1 mM DTT (pH 8.2). Resultant purified histidine-tagged Ppr is treated with Factor Xa (Novagen) to remove histidine-linker. Purified Ppr (without histidine-tag) is obtained through the same method as mentioned above, the difference being that 50 mM imidazole was used instead in Ni Sepharose™ 6 Fast Flow column elution.

The purified H-H-Ppr was treated with hydroxylamine to obtain A-H-Ppr. Prior to hydroxylamine treatment, the process involve removal of DTT by dialysis with 25 mM Tris-HCl, 50 mM NaCl, 2% glycerol, 5 mM EDTA (pH 8.2). After that, hydroxylamine was added to the final concentration of 500 mM. The sample mixture was incubated at 20 °C and monitored with UV-Visible spectrophotometer until the absorbance peak at 430 nm was completely disappeared. Bleached Ppr was dialyzed in 25 mM Tris-HCl, 50 mM NaCl, 2% glycerol, 5 mM EDTA and 1 mM DTT (pH 8.2) to remove hydroxylamine.

#### 2.2.2 UV-Visible spectroscopy

UV-visible spectra were recorded using QE65000 spectrometer (Ocean Optics, USA). Buffer condition used was 25 mM Tris-HCl, 50 mM NaCl, 2% glycerol and 5 mM EDTA (pH 7.0). A-H-Ppr and H-A-Ppr contains additional 1 mM DTT to stabilize the sample. Temperature of the cell holder is maintained at 20 °C. Sample irradiation light source is blue LED ($\lambda_{max}$ = 470 nm) and red LED ($\lambda_{max}$ = 630 nm). Before absorption spectrum measurements were carried out, Ppr sample was pre-irradiated with red light for 30 minutes and allowed to recover to dark state for 7 hours. This was carried out to ensure the measured samples were in the appropriate dark adapted form.

In order to further eliminate any contribution from fluorescence and stray scattered light from LED source, emission spectra were measured with identical parameters as absorption spectra measurements. Recorded emission spectra were subtracted from the recorded absorption spectra to obtain much more accurate representation of Ppr absorption spectra.

## 2.3 Results and Discussions

### 2.3.1 Spectroscopic properties of dark state Ppr

Figure 2-1 demonstrates the dark state absorbance spectrum for H-H-Ppr, A-H-Ppr and

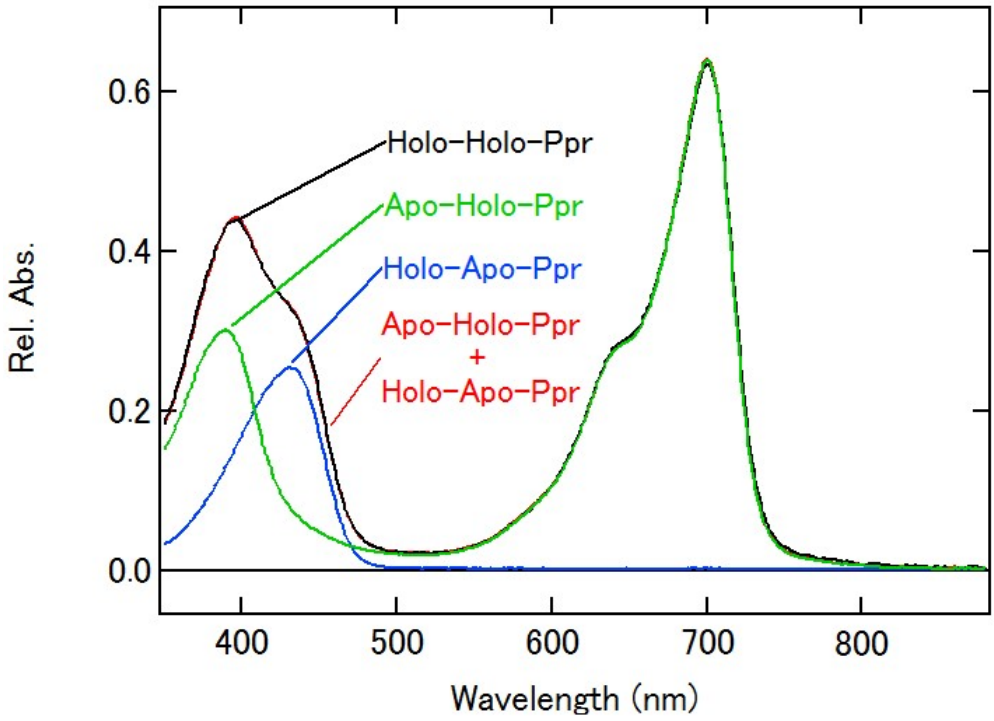


**Figure 2-1**. Absorption spectra of dark state Holo-Holo-Ppr (black), Apo-Holo-Ppr (green) and Holo-Apo-Ppr (blue). Convoluted absorption spectrum of Apo-Holo-Ppr and Holo-Apo-Ppr represented by red curve.

H-A-Ppr. A-H-Ppr which is reconstituted with BV chromophore shows characteristic peaks at 700 nm and 390 nm, while H-A-Ppr with only pCA chromophore displays its characteristic peak at 430 nm. Taking the absorption wavelength region into consideration, red light ($\lambda_{max}$ = 630 nm) is absorbed by the major absorption peak of Bph domain. Blue light irradiation ($\lambda_{max}$ = 470 nm) is absorbed by both PYP and Bph domains, though the blue light absorption efficiency is small for Bph domain compared to PYP domain. Although the same Ppr protein was used for all these three chromophore reconstitution conditions, the observation shows good agreement with the other study of similar setup (except for the usage of H-A-Ppr) (37) where H-H-Ppr dark state spectrum is a combination of the A-H-Ppr and H-A-Ppr individual dark state spectra respectively. This combination is most notably observed around 400 nm peak with a 430 nm shoulder in H-H-Ppr. Based on these information, the PYP and Bph domains in their dark state forms (hereby termed $Bph_D$ and $PYP_D$) do not affect each other within Ppr.

### 2.3.2 Spectroscopic properties of single chromophore Ppr variants, Holo-Apo-Ppr and Apo-Holo-Ppr

Figure 2-2A shows absorption spectra of H-A-Ppr in the dark and under blue light irradiation. Upon blue light irradiation, absorption spectrum decrease around 430 nm. Minor increase of absorption could be observed around 350 nm and 470 nm. The H-A-Ppr blue/dark difference absorbance spectrum features (Figure 2-2B) resembles closely to the $PYP_L$/dark difference spectrum of *Hh*-PYP (41). The most significant feature in the difference spectrum is the absorption peak round 470 nm, which corresponds to the formation of $PYP_L$ photointermediate. This signifies that H-A-Ppr which only contains pCA chromophore photoconverts from $PYP_D$ to $PYP_L$ under continuous blue light irradiation.

Figure 2-3A demonstrates the absorption spectra of A-H-Ppr in the dark and under red

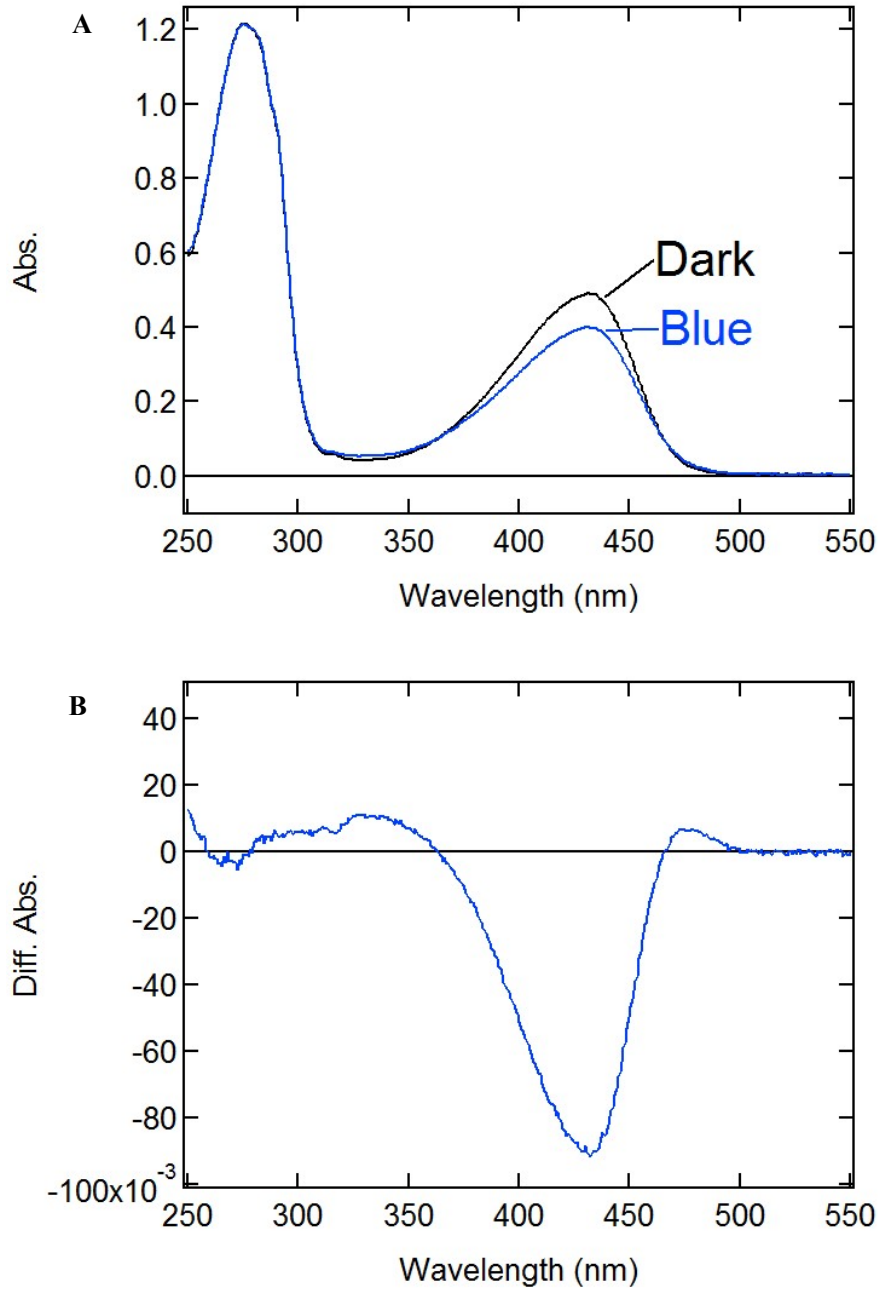


**Figure 2-2.** (A) Absorption spectra of Holo-Apo-Ppr under dark and blue light irradiation. (B) Blue/dark difference absorption spectrum of Holo-Apo-Ppr. [Detailed representation in Appendix section, Figure S1 and S2]

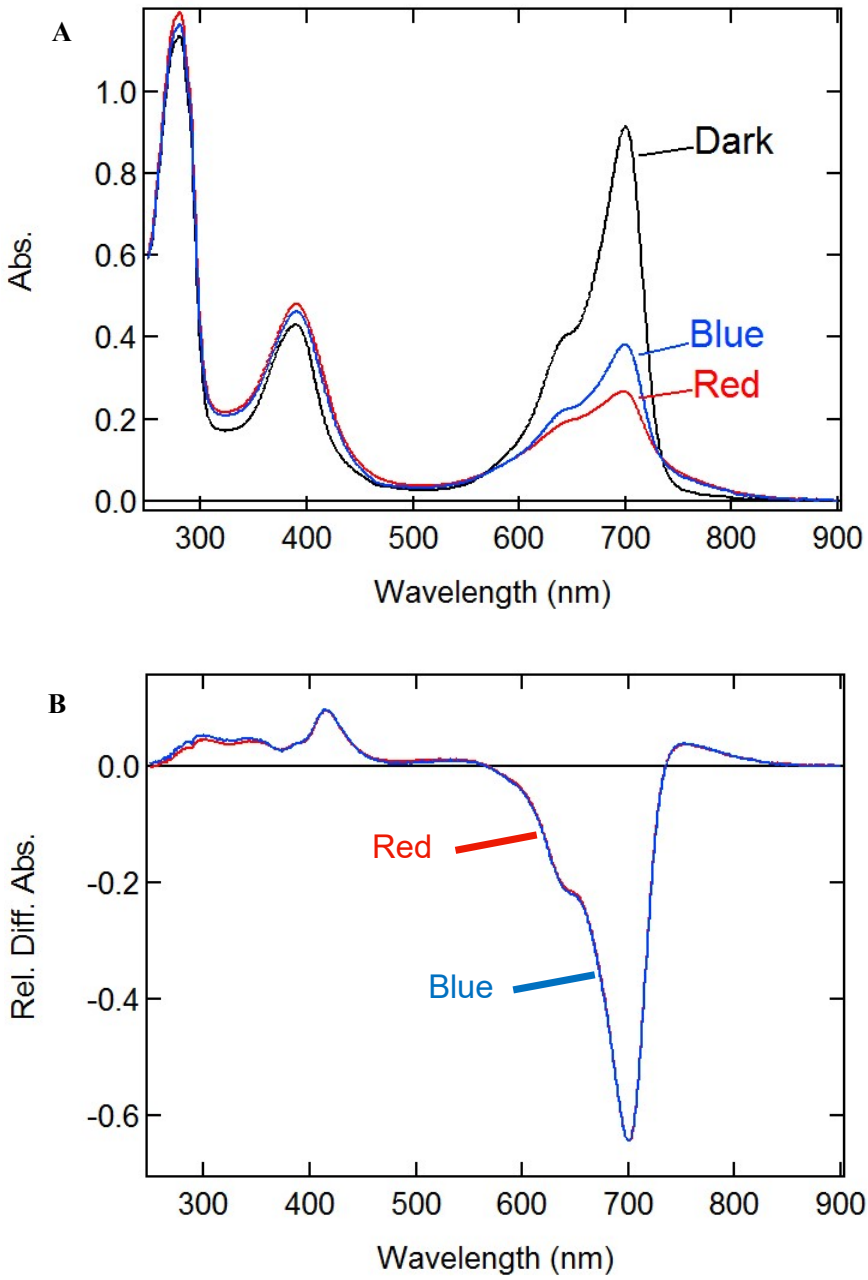


**Figure 2-3.** (A) Absorption spectra of Apo-Holo-Ppr under dark, red light irradiation and blue light irradiation. (B) Red/dark difference absorption spectrum (red) and blue/dark difference absorption spectrum (blue) of Apo-Holo-Ppr. Red spectrum normalized to blue spectrum. [Detailed representation in Appendix section, Figure S3 and S4]

light or blue light irradiation. Under light irradiation, H-H-Ppr showed that Bph spectrum around 700 nm decreases with a slight increase in the soret band region. This absorption decrease around 700 nm is the characteristic feature of the BV in Bph domain being photoconverted. It is hereby term as Bph* to represent such change. A-H-Ppr shows the strongest absorption decrease around 700 nm under red light. This is most likely due to the higher absorption efficiency by the biliverdin for red light compared to blue light. Although both red and blue light irradiation conditions results in different amount of Bph*, comparing both spectra indicates that photoproducts from both irradiation conditions are similar (Figure 2-3B). Different irradiation condition does not results in different Bph photoproduct.

### 2.3.3 Spectroscopic properties of Ppr with fully reconstituted chromophores, Holo-Holo-Ppr

Under continuous red light irradiation, H-H-Ppr shows a similar spectrum change to A-H-Ppr. Bph absorption spectrum around 700 nm decreases with a slight increase in the soret band region (Figure 2-4A). The similarity is demonstrated in Figure 2-4B which indicates A-H-Ppr under light irradiation and H-H-Ppr under red light irradiation have the same Bph* photoproducts. This information suggests that the presence of dark state pCA chromophore in H-H-Ppr does not influence the photoreaction of Bph.

Under the assumption that both pCA and BV chromophores do not interfere with each other, it was compelling to think that the convoluted difference spectra of both blue/dark of H-A-Ppr (Figure 2-2B) and red/dark of A-H-Ppr (Figure 2-3B) would be similar to red-blue/dark of H-H-Ppr. However, experimental measurements demonstrated differences exist between convoluted difference spectrum and measured red-blue/dark difference spectrum (Figure 2-5). The difference between two spectra is most prominent around 400 nm and 700 nm, attributed

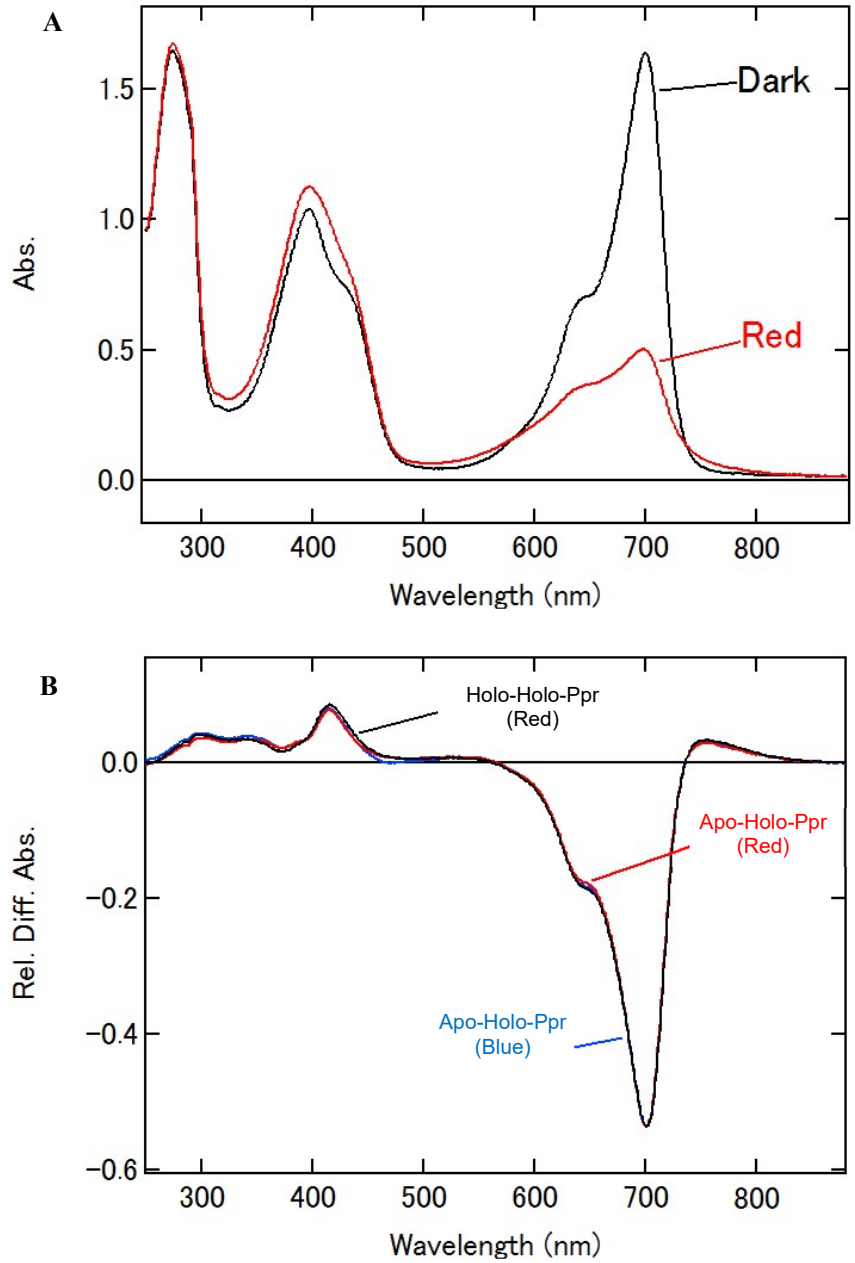


**Figure 2-4.** (A) Absorption spectra of Holo-Holo-Ppr under dark and red light irradiation. (B) Red/dark difference absorption spectrum of Holo-Holo-Ppr (black), red/dark difference absorption spectrum of Apo-Holo-Ppr (red) and blue/dark difference absorption spectrum (blue) of Apo-Holo-Ppr. Black and red spectrum normalized to blue spectrum.

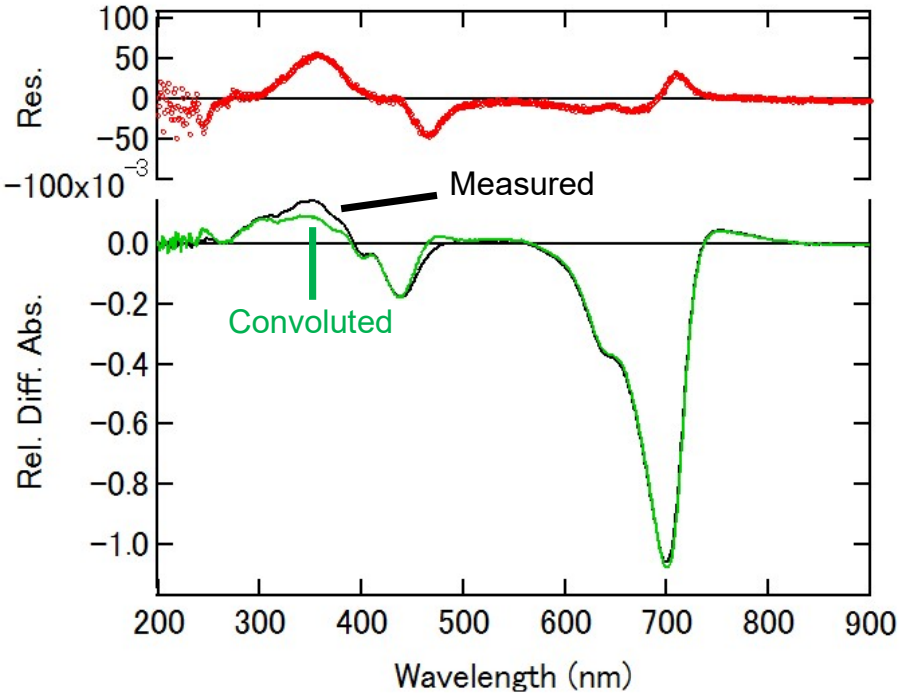


**Figure 2-5.** Red-Blue/dark difference absorption spectrum of Holo-Holo-Ppr represented by black curve. Convoluted difference spectra of both blue/dark of H-A-Ppr (Figure 2-2B) and red/dark of A-H-Ppr (Figure 2-3B) represented by green curve. Residual difference between two curves represented by red scatter marks above.

to PYP domain and Bph domain respectively. This indicates that light state H-H-Ppr where both chromophores are photoactivated undergoes different photoreactions compared to the single chromophore Ppr variants.

Under continuous blue light irradiation, H-H-Ppr shows an increase of absorbance around 350 nm and a decrease of absorbance around 434 nm (Figure 2-6A). This changes is mainly due to the photoconversion of pCA in PYP domain (PYP*). In addition, similar decreasing of absorption spectrum around 700 nm could be observed. This spectrum change around 700 nm is attributed to the photoactivation of Bph domain as the blue light also photoactivates Bph through the soret peak absorbance. Comparing the difference spectra of H-H-Ppr under blue light irradiation in Figure 2-6B to those of the single chromophore Ppr variants, the most obvious difference can be seen around 400 nm. This indicates a different photoreaction involved in PYP domain in H-H-Ppr compared to H-A-Ppr under blue light irradiation.

Upon closer inspection, the difference absorbance spectra under blue light irradiation demonstrate the absorbance initially decrease at 434 nm followed by a slight increase. This is clearly shown in Figure 2-7 where the time course of absorbance changes of 434 nm has a lowest peak around 5 minutes. The absorbance changes over time can be sufficiently fitted by a double exponential function with the time constant shown in Table 2-1. This indicates that at least two photoreactions are involved under continuous blue light irradiation. Using the 5 minute mark as the transition point of reference (Figure 2-8A), blue light irradiation time domain can be categorized into early phase and late phase. Based on these two time domains, two distinct difference absorption spectra could be obtained as shown in Figure 2-8B and

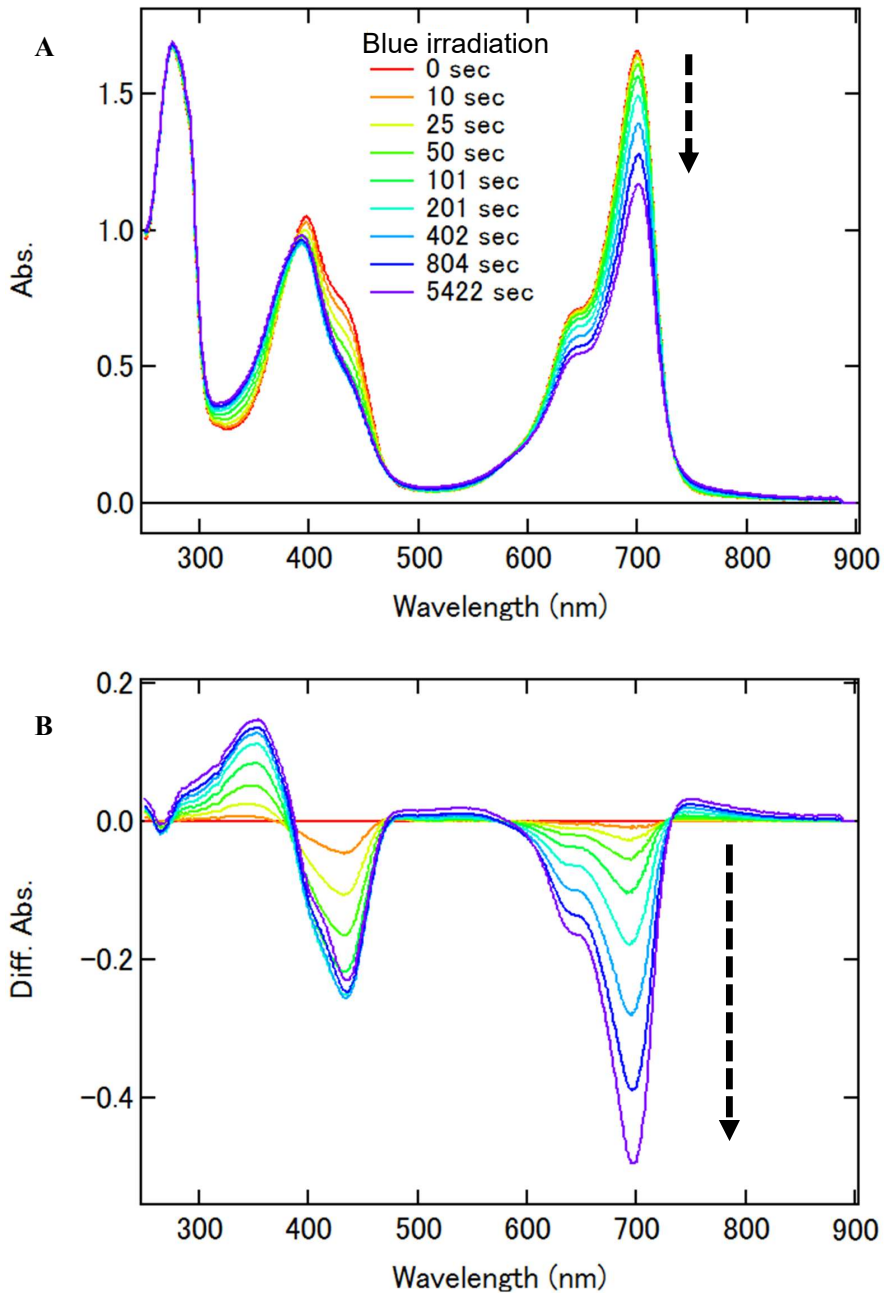


**Figure 2-6.** (A) Absorption spectra of Holo-Holo-Ppr under blue light irradiation. (B) Blue/dark difference absorption spectra of Holo-Holo-Ppr.

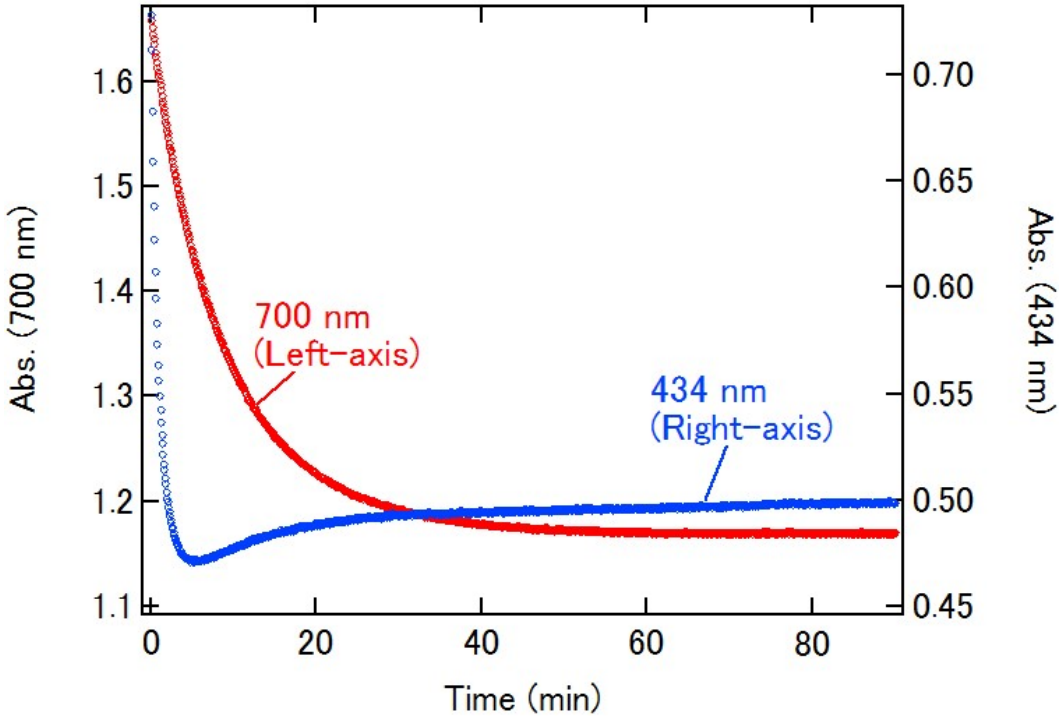


**Figure 2-7.** Time-resolved absorbance of Holo-Holo-Ppr under blue light irradiation at selected wavelength 700 nm and 434 nm from panel A at every 5 seconds interval.

**Table 2-1.** Kinetic rate constants for Holo-Holo-Ppr under blue light irradiation at selected wavelengths.

| Wavelength | Kinetic rate constant 1 ($min^{-1}$) | Kinetic rate constant 2 ($min^{-1}$) |
|---|---|---|
| 434 nm | 1.085 ± 0.005 | 0.0629 ± 0.0008 |
| 700 nm | 0.205 ± 0.002 | 0.0901 ± 0.0004 |

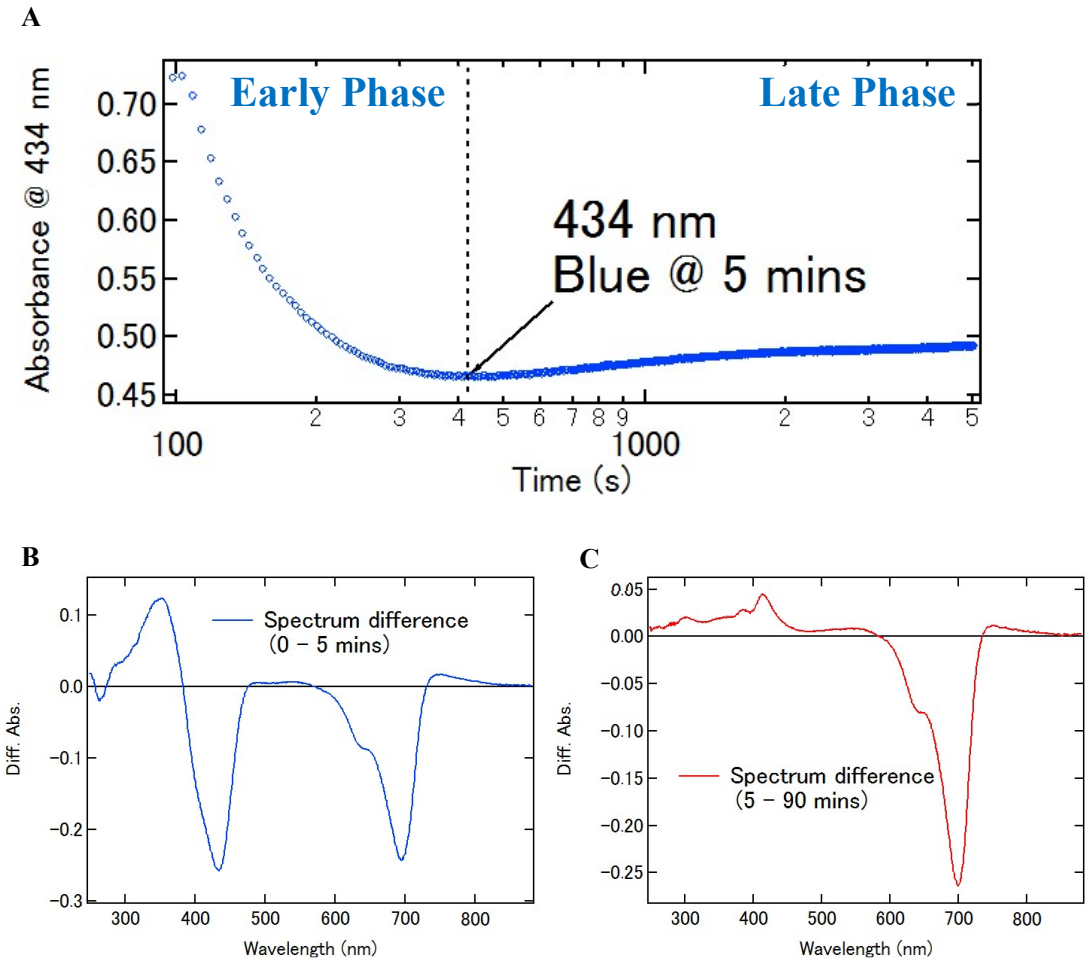


**Figure 2-8.** (A) Time-resolved absorbance of Holo-Holo-Ppr at 434 nm. Separated into early phase and late phase time domains by the 5$^{th}$ minute time point around the minimum absorbance value of 433 nm. Time axis represented in logarithmic scale to resolve early phase time domain. (B) Early phase difference absorption spectrum of Holo-Holo-Ppr under blue light irradiation between initial measurement and 5$^{th}$ minute measurement. (C) Late phase difference absorption spectrum of Holo-Holo-Ppr under blue light irradiation between 5$^{th}$ minute measurement and final measurement at 90$^{th}$ minute.

Figure 2-8C. In the early phase, spectrum changes attributed to PYP and Bph domains could be observed. In the late phase, spectrum change is mainly attributed to Bph domain which is similar to the difference spectrum features seen under red light irradiation. This clearly shows that PYP and Bph have different rate of photoreactions under blue light, with the photoreactions of PYP reaching photostationary state (PSS) followed by photoreaction of Bph. In addition, a detail comparison of the peak difference absorbance around 700 nm shows a different peak value. In the early phase, the peak shifted to 695 nm compared to the late phase or red light irradiation which has the peak spectrum at 700 nm. It shows a sign of chromophore environment change of Bph domain occurs within early phase of blue light irradiation.

### 2.3.4 Holo-Holo-Ppr in early phase blue light irradiation

As the photoreaction in the early phase blue light irradiation of H-H-Ppr is seemingly complex involving at least two photoreactions with different kinetics, a variation of time-dependent difference spectra was performed to better analyze the early photoreaction phase (Figure 2-9A). Difference spectra between each measurements over time were plotted to allow a clear visualization on the changes of difference spectrum during the course of blue light irradiation. The time interval was chosen at 5 seconds which has sufficient time resolution while maintaining a good signal-to-noise ratio.

It is discovered that in the initial 10 seconds of blue light irradiation (Figure 2-9B), the difference spectrum closely resembles to that of the H-A-Ppr under blue light irradiation. The spectrum feature around 400 nm is also similar to Ppr-PYP (truncated Ppr with only PYP domain) and His-Ppr (histidine-tagged Holo-Apo-Ppr configuration) under continuous blue light irradiation reported in the previous study (40). The absorbance peak around 470 nm diminishes within 30 seconds of continuous blue light irradiation (Figure 2-9C). Furthermore,

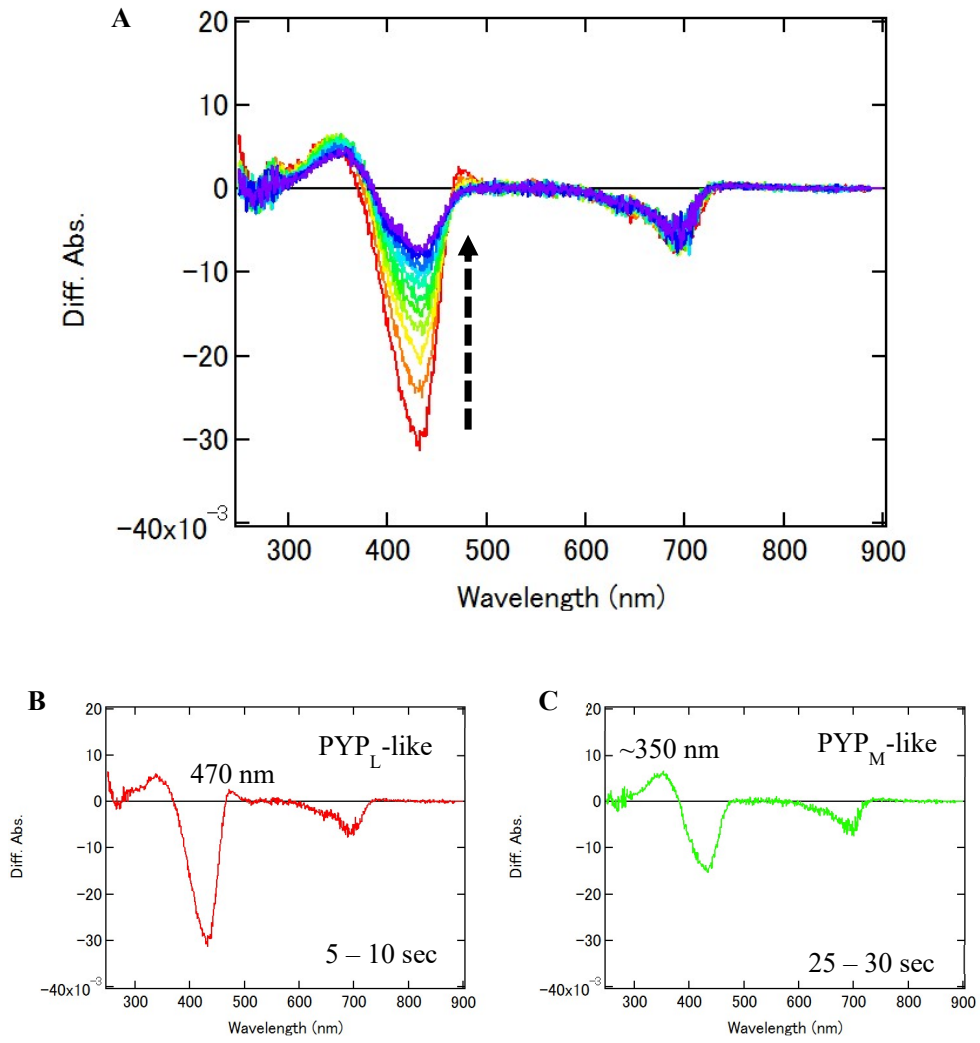


**Figure 2-9.** (A) Absorption difference spectrum of Holo-Holo-Ppr at 5 seconds difference interval under blue light irradiation (5 sec – 60 sec, red to blue curves). Two distinct PYP related spectra shown in 5 – 10 sec difference (B) and 25 - 30 sec difference (C).

the absorbance ratio of 350/434 nm increases over the course of blue light irradiation. All these changes can be clearly seen in the series of images in Figure 2-10. The absorbance changes in the early phase of blue light irradiation indicates the formation of $PYP_L$ and $PYP_M$ photointermediates, analogous to the changes in *Hh*-PYP (31). Another reference with similar observations can be found in the study of Ppr-PYP (40).

The spectral changes around 400 nm in Figure 2-9 does not accurately represent the photoreactions involved in PYP considering the early blue light irradiation phase includes spectral contribution from Bph (refer Figure 2-4B). In order to allow a more precise analysis, the spectral contribution of Bph needs to be removed. The absorption difference spectrum of H-H-Ppr at 700 nm under continuous blue light irradiation beyond 5 minutes has similar difference spectrum to that of under continuous red light irradiation (Figure 2-8C), with peak difference spectrum at $\lambda_{max}$ = 700 nm. Assuming the difference spectrum from Bph photoreaction is also similar around 400 nm region, the H-H-Ppr red/dark difference spectrum from red light irradiation is used as the basis to subtract the Bph spectrum contribution from the blue light irradiation difference spectrum, obtaining a difference spectrum which approximate closely to photoreaction of PYP domain (Figure 2-11A & Figure 2-12A). The Bph subtracted difference spectra are compared with the difference spectrum of H-A-Ppr under continuous blue light irradiation.

A comparison of the Bph subtracted difference spectrum of H-H-Ppr (5 - 10 seconds) and H-A-Ppr at blue light PSS (Figure 2-11B) shows a good agreement between 2 difference spectra around 434 nm and 470 nm. In a similar comparison, difference spectrum of H-H-Ppr (25 – 250 seconds) shows a higher absorbance at 350 nm and absence of absorbance peak at 470 nm (Figure 2-12B). This signifies that for H-H-Ppr under blue light irradiation, the initial

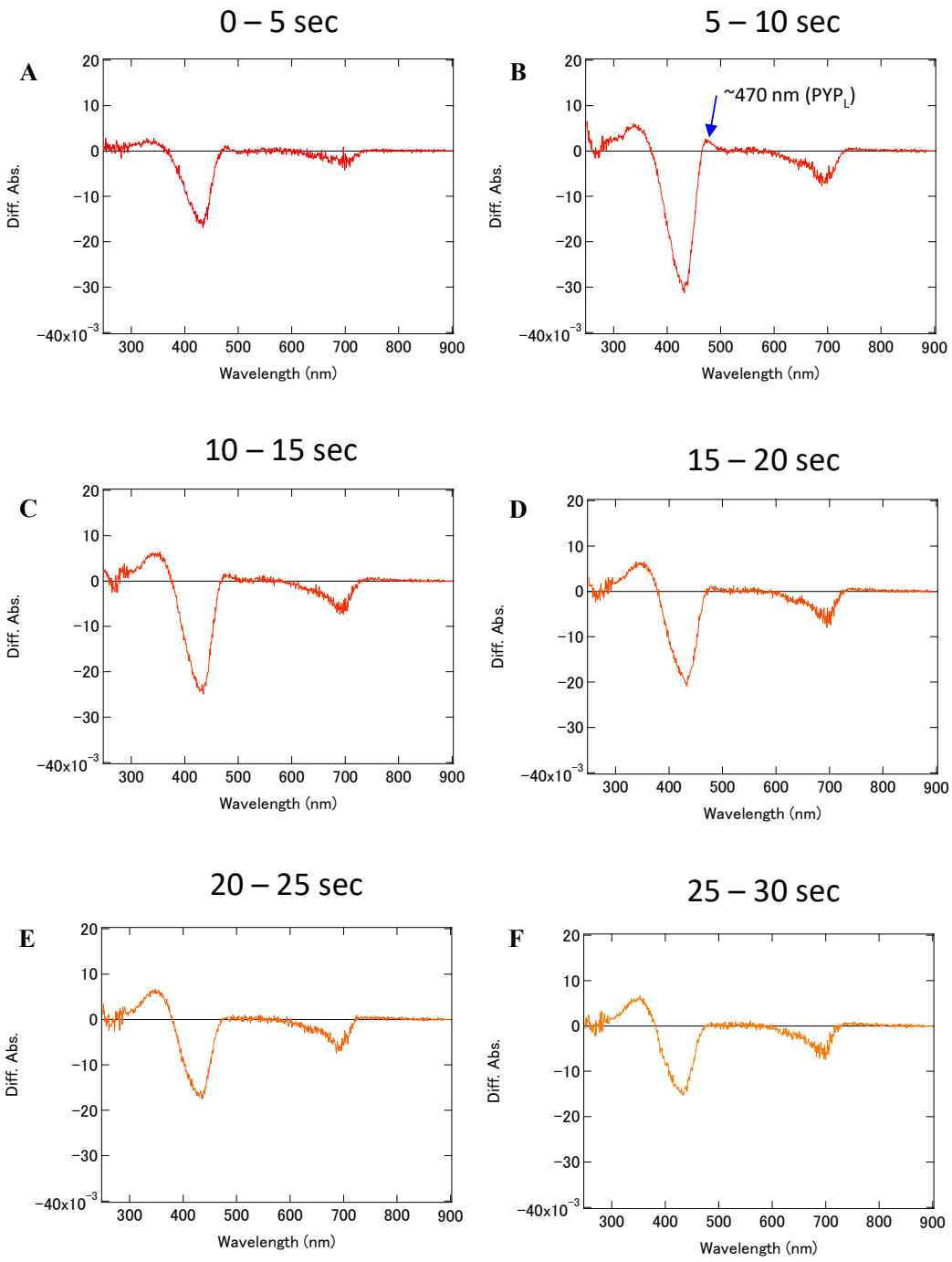


**Figure 2-10.** Time resolved difference spectra of Holo-Holo-Ppr at every 5 seconds difference interval under blue light irradiation (0 sec – 30 sec). Small peak indicated by blue arrow at 470 nm only observable for the initial 20 seconds of blue light irradiation.

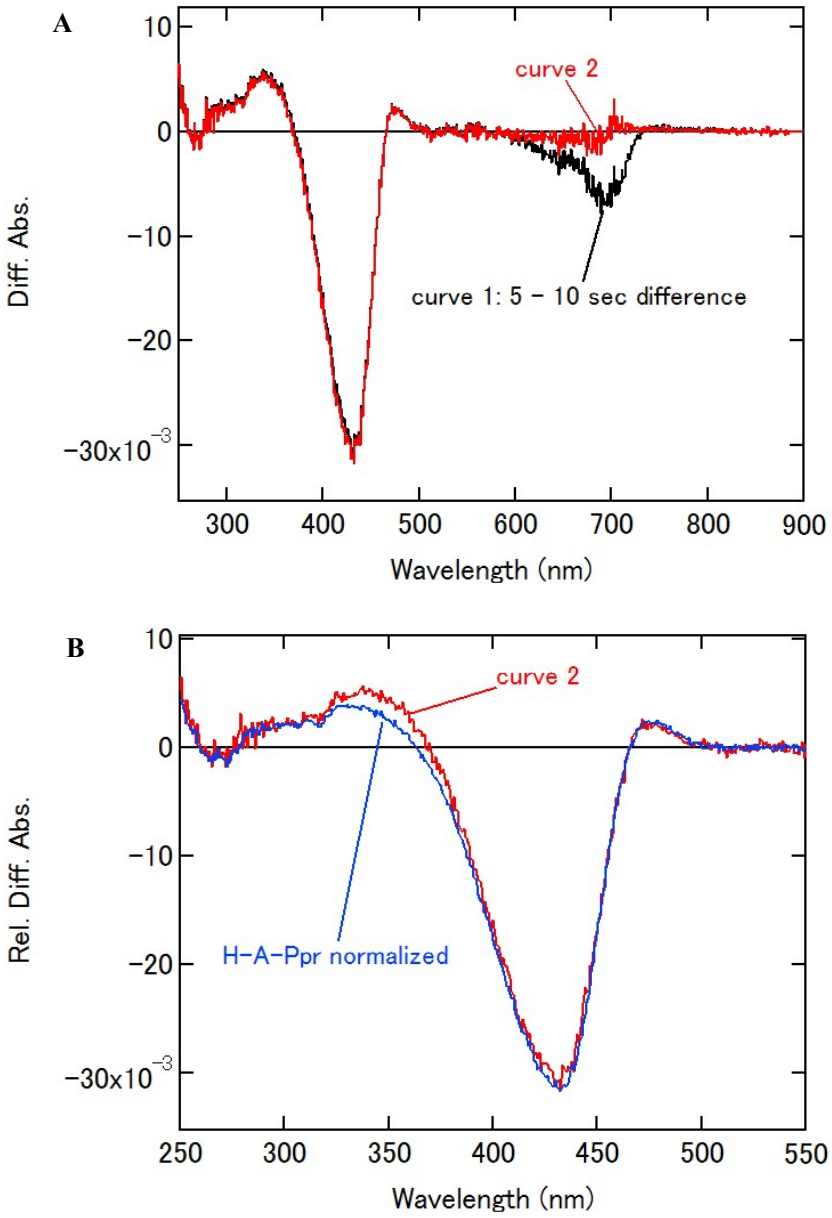


**Figure 2-11.** (A) Curve 1 represents the absorption difference spectra between 5 and 10 seconds blue light irradiation of Holo-Holo-Ppr, similar to Fig. 2-10B. Red/dark difference spectrum of Holo-Holo-Ppr after 30 minutes red light irradiation (Fig. 2-4B) is normalized and subtracted from curve 1, resulting in curve 2. (B) Blue/dark difference spectrum of Holo-Apo-Ppr is normalized and superposed with curve 2.

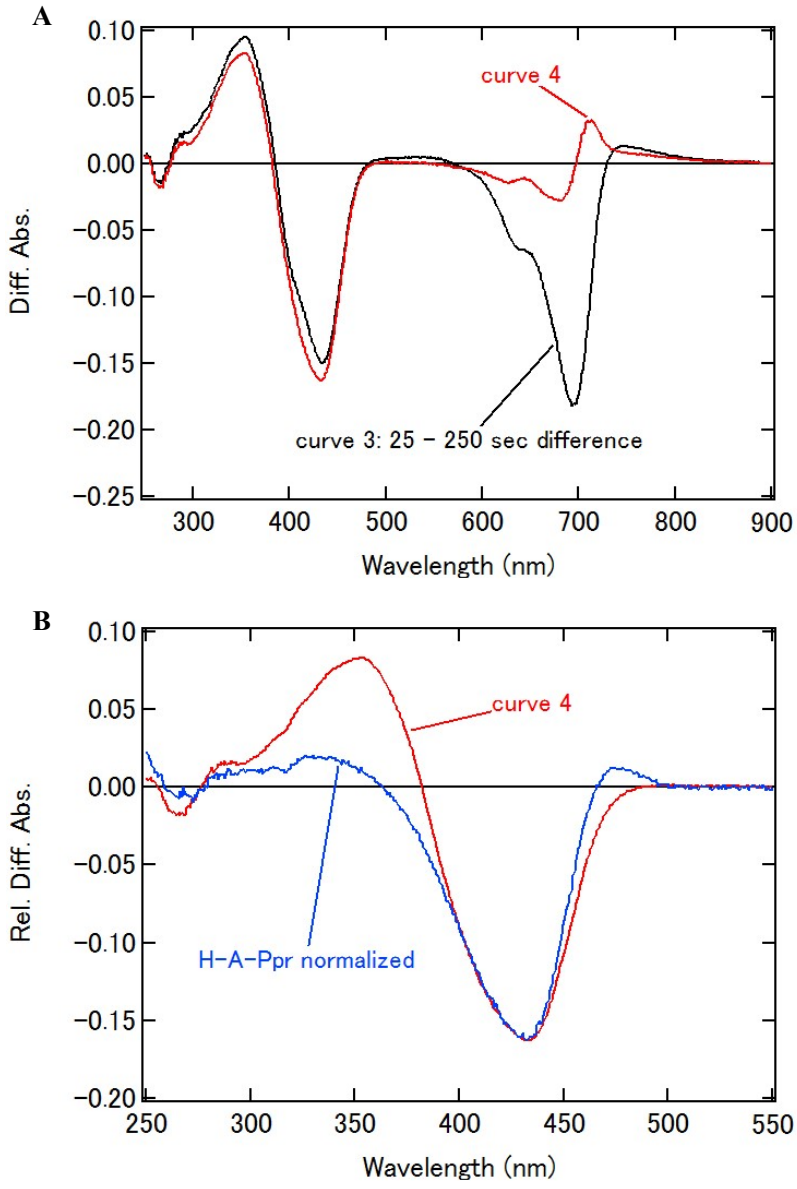


**Figure 2-12.** (A) Curve 3 represents the absorption difference spectra between 25 and 250 seconds blue light irradiation of Holo-Holo-Ppr Red/dark difference spectrum of Bph after 30 minutes red light irradiation (Fig. 2-4B) is normalized and subtracted from curve 3, resulting in curve 4. (B) Blue/dark difference spectrum of Holo-Apo-Ppr is normalized and superposed with curve 4.

photoreaction is similar to H-A-Ppr. This initial photoreaction within the first 10 seconds of blue light involves formation of $PYP_L$ photointermediate. However, the presence of BV in H-H-Ppr seems to stabilize the formation of $PYP_M$ photointermediate. This results in $PYP_M$ being accumulated when H-H-Ppr exposed to longer duration of blue light irradiation. It is also observed that spectrum shift around 700 nm is revealed when Bph spectral contribution is removed. In Figure 2-13, it is clearly shown that the Bph spectrum shift is larger at the later part of early phase blue light irradiation, the time domain where $PYP_M$ is accumulated. This suggests formation of $PYP_M$ influence the Bph domain, possibly the chromophore environment of BV. In order to verify the influence is indeed from $PYP_M$, difference absorbance changes from various time points that represents $PYP_M$ formation (350 nm) and Bph wavelength shift (710 nm) are sampled (Figure 2-14A) and compared. Figure 2-14B demonstrates the kinetic rate between $PYP_M$ formation and Bph wavelength shift are comparable to each other. In contrast to the kinetic rate of the Bph* formation under blue light irradiation which is noticeably slower. This shows that Bph domain do indeed influenced by formation of $PYP_M$.

### 2.3.5 Summary

Figure 2-15 summarize the photoreaction schemes in this chapter. This study found that dark state chromophores does not influence each other in H-H-Ppr (S1). In addition, presence or absence of dark state pCA chromophore does not results in any changes to photoreaction of Bph (S2). However, blue light irradiation which photoactivates both pCA and BV results in different photoreactions in H-H-Ppr compared to the single chromophore Ppr variants (S3). Most importantly in the early phase of blue light irradiation, it is revealed that PYP domain and Bph domain mutually influence to each other. The presence of BV chromophore in H-H-Ppr promotes formation of $PYP_M$ in addition to $PYP_L$. This is evident by the initial photoreaction is similar to that of H-A-Ppr in $PYP_L$ formation, and further blue light irradiation indicates

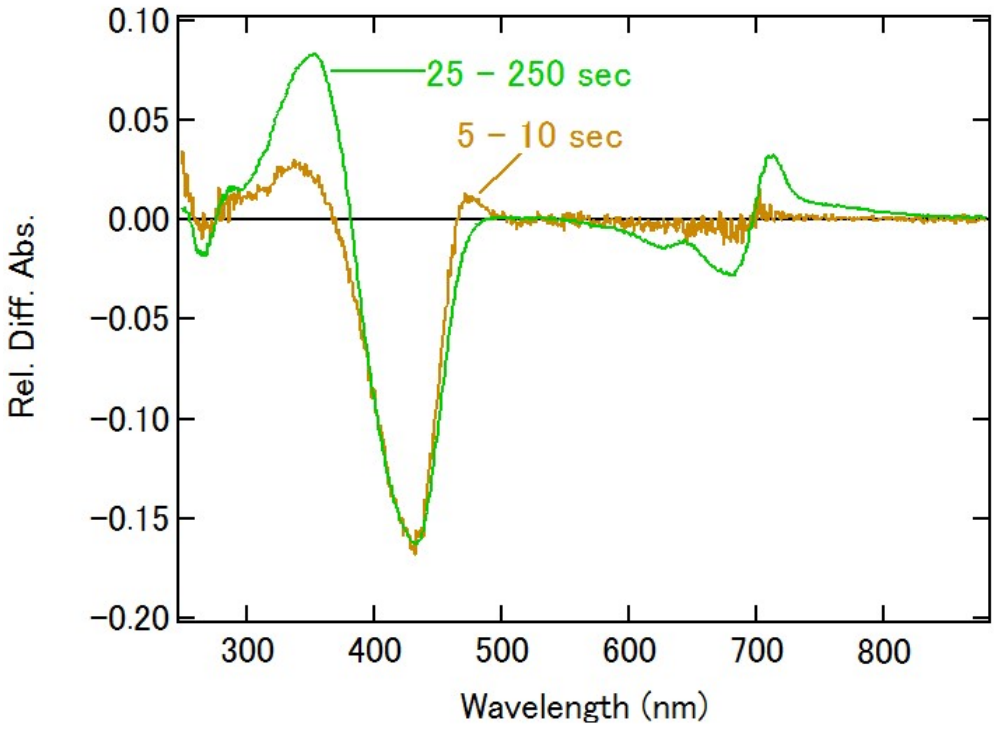


**Figure 2-13.** Absorption difference spectra Holo-Holo-Ppr under blue light irradiation between 5-10 seconds irradiation (brown) and 25-250 seconds irradiation (green). Bph spectral contribution removed from both spectra.

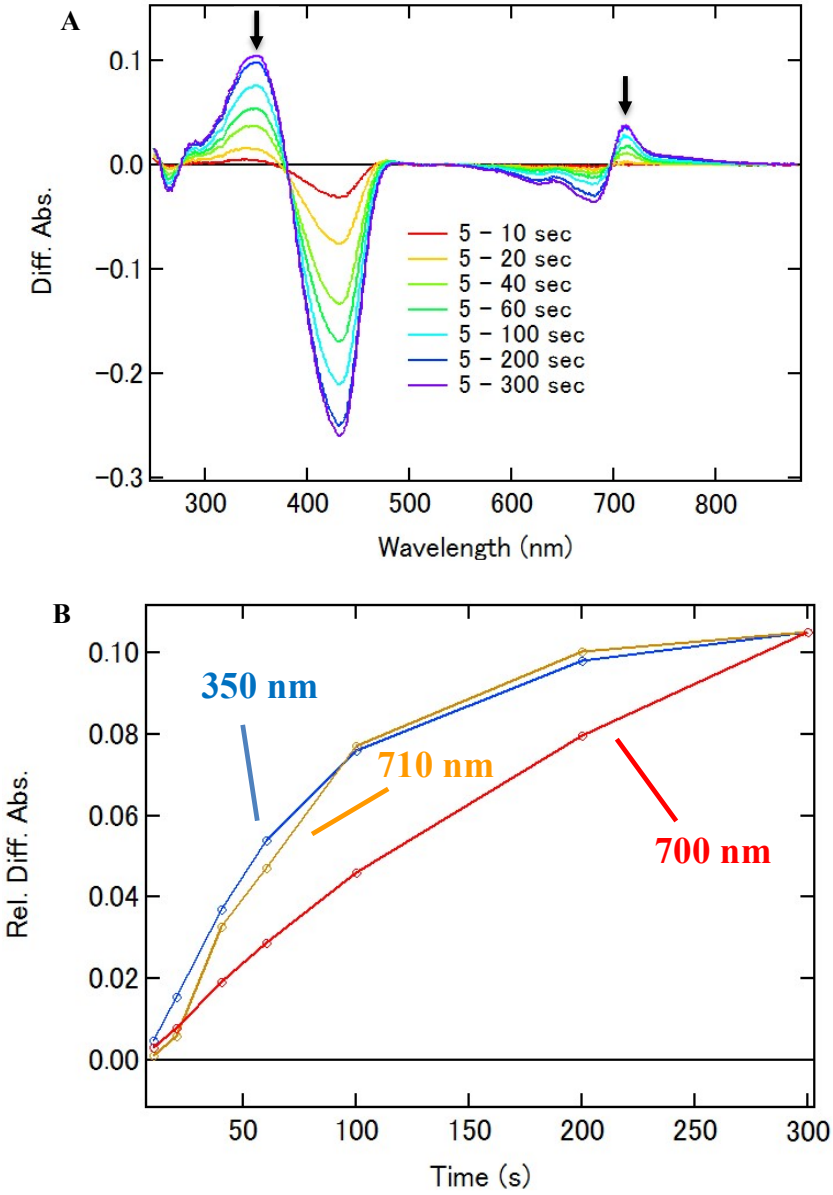


**Figure 2-14.** (A) Absorption difference spectra Holo-Holo-Ppr under blue light irradiation sampled at different time difference. Black arrow indicates the 350 nm and 710 nm wavelength points used for difference absorbance vs time in panel B. (B) Difference absorbance vs time of selected wavelength at 350 nm, 710 nm and 700 nm. Difference absorbance value of 700 nm sampled from Bph* difference spectrum used for Bph spectral contribution removal.

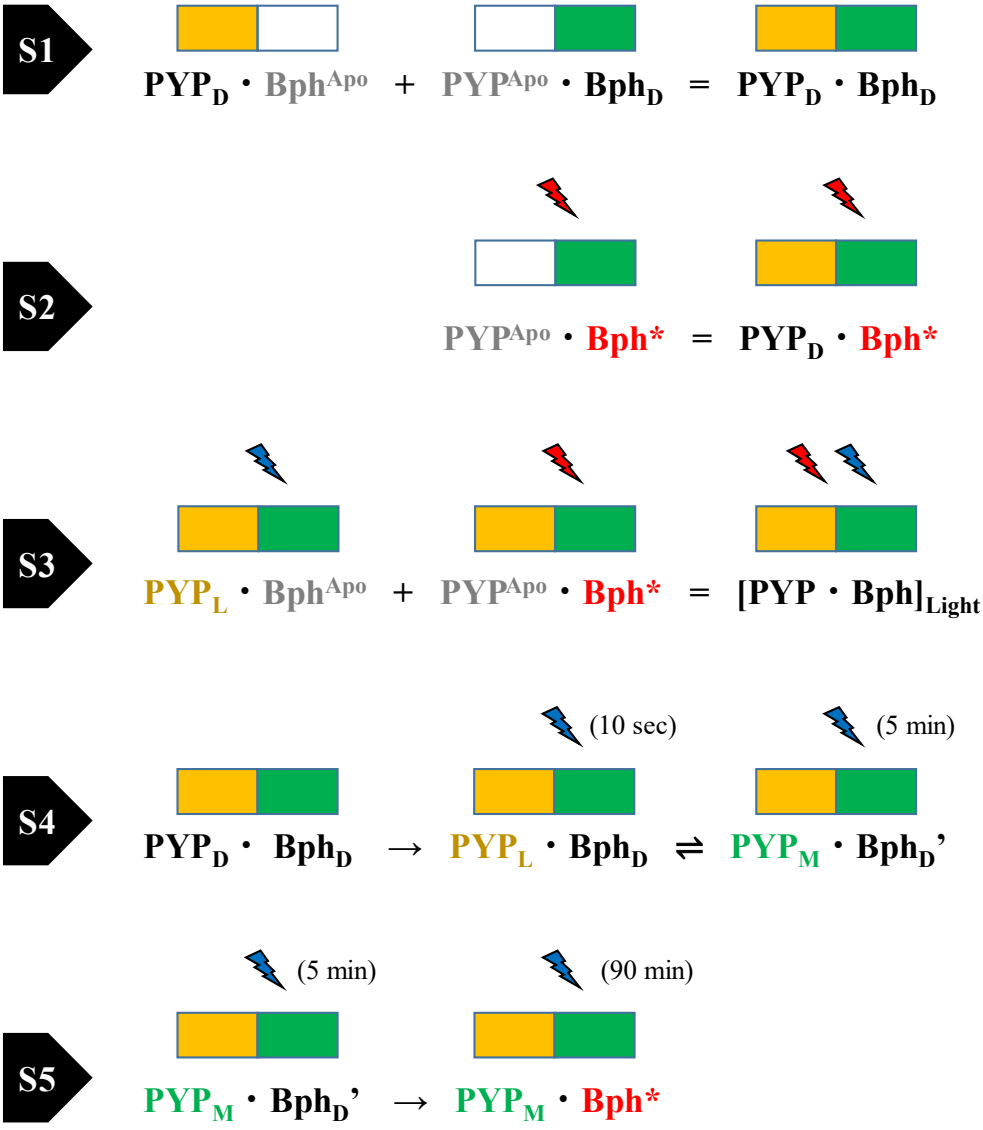


**Figure 2-15.** Photoreaction schemes of Ppr

accumulation of $PYP_M$ photoproduct. It is speculated the BV chromophore helps to stabilize the photoproduct of $PYP_M$. As the $PYP_M$ photoproduct is accumulated, Bph domain is influenced by experiencing spectrum shift around 700 nm. This phenomenon could be interpreted as a sign of BV chromophore environment being perturbed. While all the photoreactions surrounding PYP domain unfold, Bph domain which is also capable of absorbing blue light undergoes photoreaction in parallel at a slower kinetic rate. This results in the late phase of blue light irradiation, only photoreaction of Bph is observed. In the late phase time domain, PYP domain has already achieved PSS. In brief, the early phase of blue light irradiation sees a major increase in $PYP_M$ photoproduct (S4). The late phase of blue light irradiation mostly involves the increase in Bph* photoproduct (S5).

Considering $PYP_M$ influence chromophore environment of Bph in early phase of blue light irradiation, it can be thought that structural change is involved between dark state and blue light state Ppr. One of the possibility involves the spatial location changes between PYP and Bph domain that affects the chromophore environment of Bph. This structural information of Ppr is to be investigated in the following chapter.

## CHAPTER 3: Structural Aspects of Ppr

### 3.1 Background

In the protein signaling pathway, an activated protein that triggers downstream reactions is almost always accompanied by a structural change in the protein tertiary structure. An example of this is observed in *Hh*-PYP under blue light irradiation. In the previous chapter, it is shown that Ppr produces several different photointermediates depending on the types of light irradiation such as Bph* with red light; $PYP_M$ and Bph* with blue light. However, spectroscopic measurements only reveals the chromophore's local environment. In order to investigate which photointermediates could be the active form of Ppr, structural information of Ppr photointermediates is needed. Here, using SAXS measurements could offer to elucidate the overall structural conformation of Ppr in terms of size and shape.

Small angle X-ray scattering (SAXS) is a technique utilized to probe the structural information of a studied sample. It has been used in studying biological samples as early as in the 1950s and much improvement to the technique has been developed ever since then. SAXS is attractive in terms of its relative simplicity in sample preparation compared to other optical based microscopy techniques. All that is needed in sample preparation is a highly purified protein sample and a suitable buffer to provide sufficient sample to buffer contrast ratio (42, 43).

Up until now, there is no direct structural information of Ppr. The closest reference would be independent X-ray crystallography structural information of PYP, Bph or HK domains based from other bacterium species (33, 44, 45). In the first part of the study, the aim is to obtain a low-resolution solution structural data of Ppr. The resulting molecular envelope would be used as a reference to manually fit and estimate the relative spatial location of each domains.

Coupled with the available spectroscopic data as reference, solution SAXS measurement was carried out on variants of Ppr under red or blue light irradiation conditions to probe the tertiary structure of light irradiated Ppr against dark state Ppr. The second part of the experiment aims to provide valuable information in which condition the Ppr undergoes any large tertiary structural changes, offering clues to the Ppr configuration responsible for its signaling state.

## 3.2 Experiments

### 3.2.1 Data collection

*Photon Factory.* SAXS data of the H-H-Ppr protein were collected at beamline BL-10C in the Photon Factory. X-ray diffraction patterns were recorded using PILATUS3 2M (Dectris) detector at wavelength of 1.488 Å. Sample-detector distance was set at 931.2 mm. Cell temperature was maintained at 19.5 °C. Sample buffer condition was 25 mM Tris-HCl, 50 mM NaCl, 2% Glycerol, 5 mM DTT and 5 mM EDTA. The exposure time was 5 minutes with each individual measurements at 10 seconds interval. Purified Ppr protein concentration used were 8.4 mg/mL, 5.6 mg/mL and 2.8 mg/mL.

*Lab SAXS*. SAXS data of the A-H-Ppr and H-A-Ppr proteins were collected within NAIST facility. X-ray source was generated by ultraX 18 (RIGAKU) generator and diffraction patterns were recorded using XII-CCD (HAMAMATSU). Cell temperature was maintained at 20 °C. Sample buffer condition was 25 mM Tris-HCl, 50 mM NaCl, 2% Glycerol, 1 mM DTT and 5 mM EDTA for both A-H-Ppr and H-A-Ppr. Purified Ppr protein concentration used for A-H-Ppr were 5.6 mg/mL, 3.7 mg/mL and 1.9 mg/mL; H-A-Ppr was 1.3 mg/mL.

### 3.2.2 Data processing

Data is processed and analyzed using Igor software (WaveMetrics). Sample measurements were

screen for radiation damage to determine the range of usable data. Kratky plot is prepared to identify "foldedness" of the sample protein. Guinier analysis was performed to obtain two SAXS invariants, the radius of gyration ($R_g$) and extrapolated intensity at zero scattering angle [I(0)]. Guinier fitting can be approximated with the following formula:

$$\ln I(q) = \ln I(0) - (R_g^2/3)\, q^2$$

Porod volume, P(r) distribution functions and $D_{Max}$ were estimated using PRIMUS program from the ATSAS suite. Based on the I(0) values obtained from Guinier fitting and P(r) distribution function, molecular weight of the Ppr sample was estimated by using I(0) of ovalbumin as the standard reference. Estimated molecular weight values was used to confirm the oligemeric status of Ppr in solution.

### 3.2.3 *Ab initio* modeling

The low-resolution ab initio modeling can be done using DAMMIN program (46). It requires an input data with real space information which is Fourier transformed from the reciprocal space data obtained from SAXS measurements. DAMMIN program serves to reconstruct a low-resolution shape filled with dummy atoms and find a configuration that closely fits the original input data. In general, approximately ten to twenty models are simulated to obtain enough population of randomly generated models that fits the experimental input data. A single P(r) distribution function curve could be equally fitted by multiple different model shape due to local minimum fit. To assist in determining which of the model has the highest likelihood of being the correct average structure, one method is to group models of similar overall shape into their own clusters. DAMCLUST program runs an algorithm that groups similar models into clusters and compares between them to allow assessment to the ambiguity of modeling result (47). The cluster with the most population members and a sound goodness-of-fit is ground enough to be chosen as the representative for re-simulation using DAMMIN. The models of the

chosen cluster are subjected to DAMAVER program to generate an averaged probability map (48). A DAMSTART file is then generated based on the averaged DAMAVER model with a modification to include a fixed core for the DAMMIN program to refer as initial guess. New models generated from DAMMIN with DAMSTART file as initial approximation are subjected to evaluation before being utilize as the final envelope model. All 3D models were visualized using Chimera v1.13.

## 3.3 Results and Discussions

### 3.3.1 *Ab initio* modeling of Ppr

Kratky plot analysis, as shown in Figure 3-1, indicates dark state H-H-Ppr assumes a multidomain structure as evident by the presence of multiple pronounced peaks around low Q region. In addition, value in the high Q region approaching towards Q-axis indicates H-H-Ppr is well folded. Guinier analysis in Figure 3-2 indicates the H-H-Ppr used in the SAXS measurement has minimal to no presence of molecular aggregation or repulsion. P(r) distribution function of H-H-Ppr estimates the Ppr maximum size at 245 Å (Figure 3-3). Molecular weight estimation based on the data from Guinier fitting and P(r) plot confirms that the solution structure measured by SAXS is in dimeric form (Table 3-1).

In total of twenty models were simulated using DAMMIN program. The simulation is done in slow mode, using parameters as shown in Table 3-3. However not all of the simulated models similar to each other. DAMCLUST program successfully group the 20 models into 8 clusters (Figure 3-4) of similar shapes, except those with no similar partners in their own individual isolated cluster. Considering that model shape from cluster 7 has the most number of members that fits the measured SAXS data, this group is considered to have the best approximation to Ppr solution structure. Additional 3 new models were simulated base on the

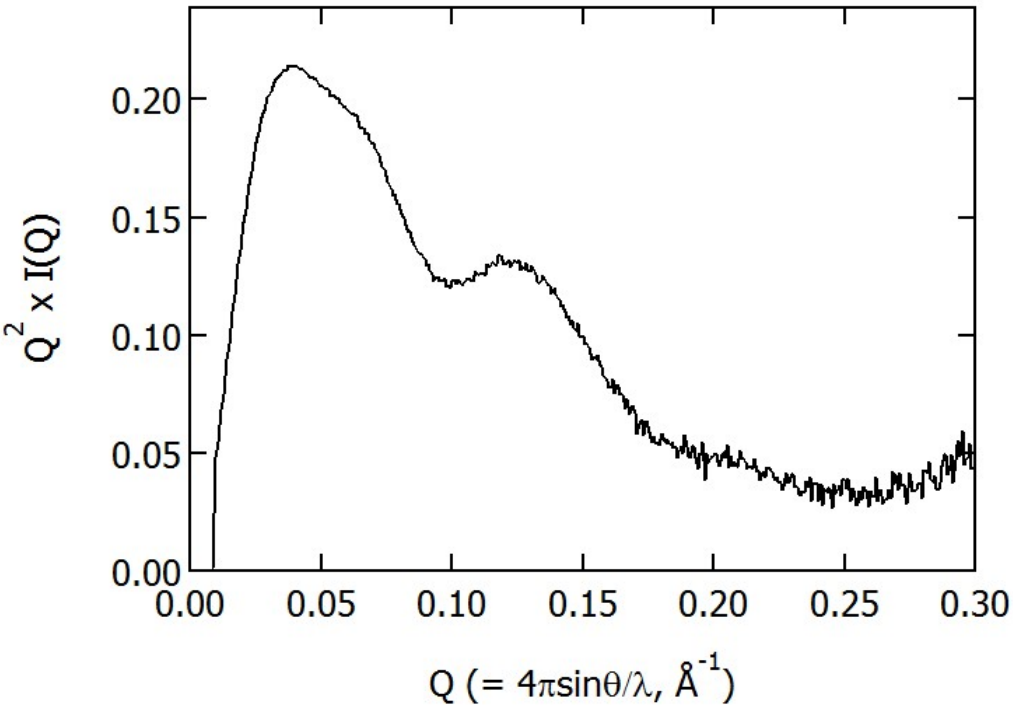


**Figure 3-1.** Kratky plot of Holo-Holo-Ppr, indicating a folded protein with multidomain structure (multiple pronounced peaks) and relatively well folded (close to x-axis at high Q region).

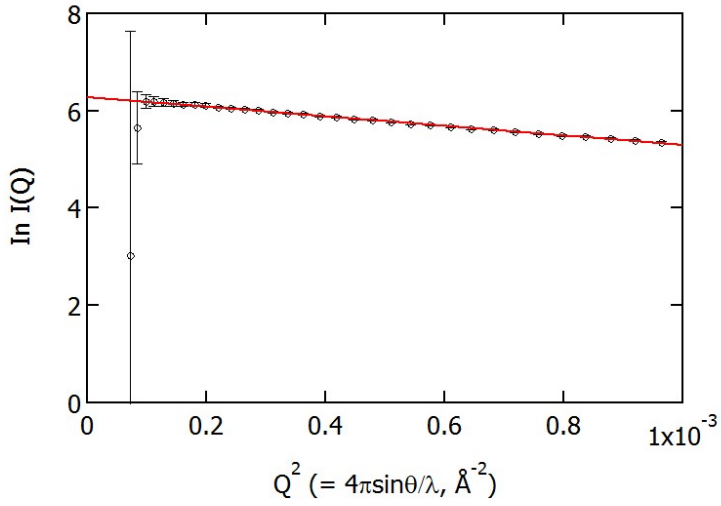


**Figure 3-2.** Guinier plot for dark state H-H-Ppr at 1.85 mg/mL.

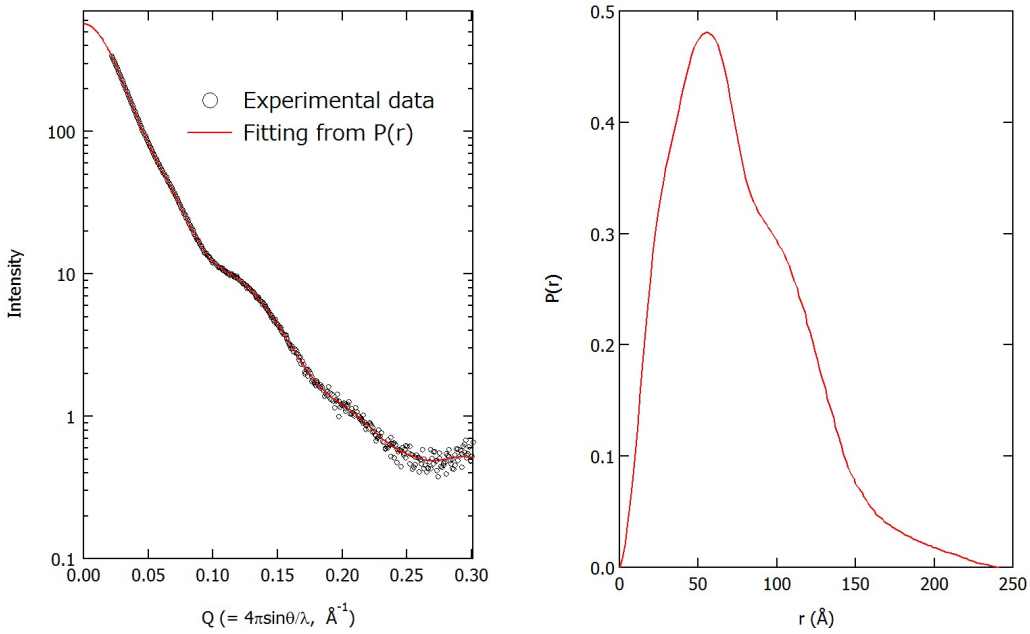


**Figure 3-3.** The left figure shows the intensity curve of experimental SAXS data from dark state H-H-Ppr and a fitting curve calculated from P(r) distribution function. Figure on the right is the Fourier transform of SAXS measurement to P(r) distribution function with $D_{Max}$ = 245 (PRIMUS program).

| | Rg (Å) | I(0)/conc. | MW (kDa) | Oligomeric units* |
|---|---|---|---|---|
| **Guinier plot (Igor)** | 54.3 ± 0.02 | 288 ± 1 | 240.9 | 2.5 |
| **P(r) plot (PRIMUS)** | 60.6 | 307.5 | 257.0 | 2.7 |

*H-H-Ppr monomer MW: 95 kDa

**Table 3-1.** The radius of gyration and forward scattering intensity of dark state H-H-Ppr from titrated SAXS measurement. Molecular weight estimation indicates solution structure of H-H-Ppr is a dimeric form.

| DAMMIN Parameters | Details |
|---|---|
| **Computation mode** | Slow |
| **Maximum diameter** | 245.0 Å |
| **Radius of gyration** | 60.46 |
| **Symmetry** | P2 |
| **Expected particle shape** | Unknown |

**Table 3-2.** Parameters used in DAMMIN simulation that requires manual input. Default program values are used for other parameters.

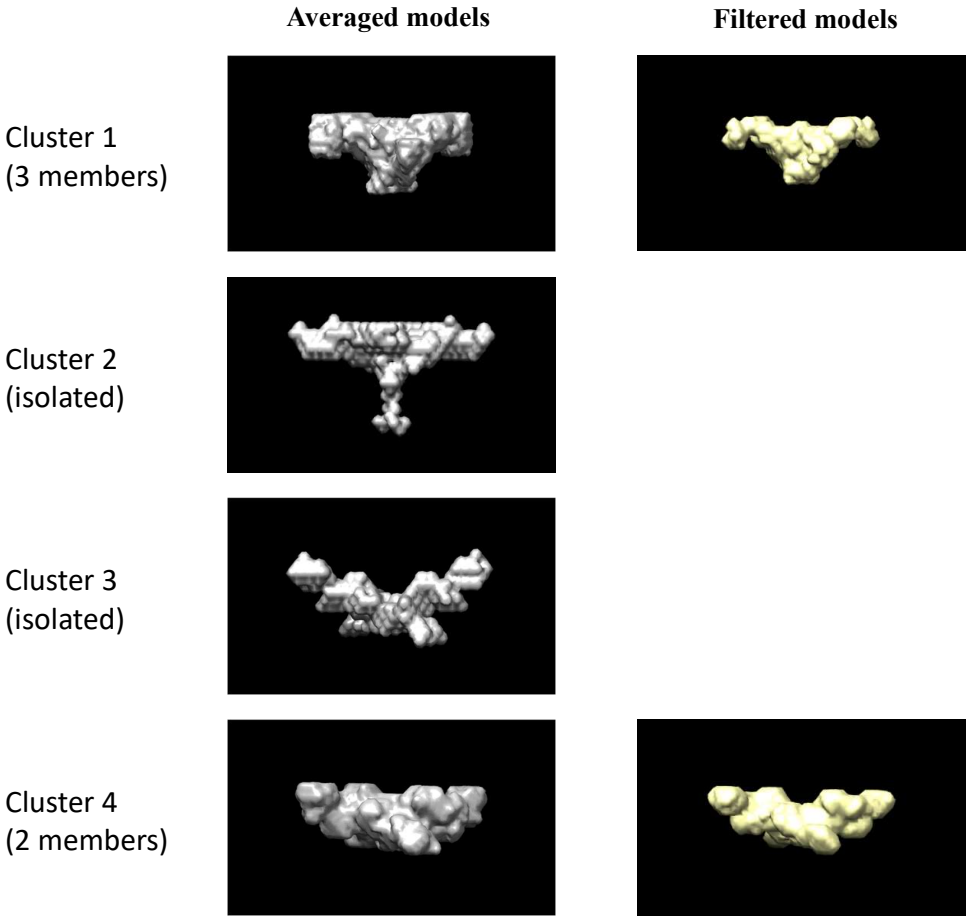


*Figures continued on next page

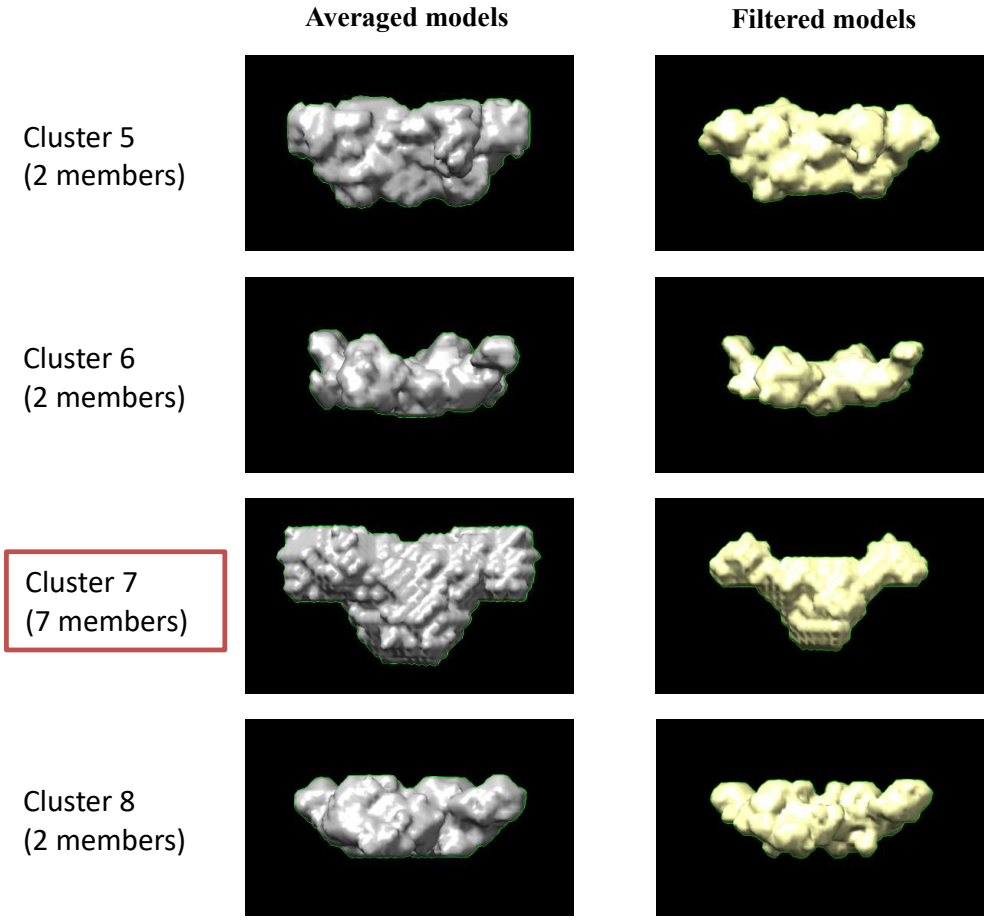


**Figure 3-4.** 8 cluster grouping from 20 simulated models. Cluster 7 has the most number of members with similar simulated model.

averaged models of cluster 7 as initial guess to fit the SAXS measurement. The three new models show good agreement with each other, taking on an open Y-structure (Figure 3-5).

X-ray crystallographic data of protein domains homologous to Ppr were obtained from protein data bank in order to manually superpose with the protein envelope acquired from *ab initio* modeling. The reference domains used are PYP from *Halorhodospira halophila* (PDB code: 2ZOI), Bph from *Deinococcus radiodurans* (PDB code: 4Q0J) and HK from *Thermotoga maritama* (PDB code: 2C2A). Filtered model of cluster seven from Figure 3-4 is used as a guidance to visually determine the relative spatial location of the core structures. Histidine kinase protein family is generally a dimeric protein. Based on this information, the domain reconstruction principle is the HK domain provides the dimerization domain with its alpha helix chains holding two Ppr monomers together at the center. The Bph domain fills the remaining space of the outer open end of the envelope. As for PYP domain, the location remains undetermined as there are multiple available empty pockets to accommodate it. However, from the protein sequence it is link to N-terminal of Bph domain via a chain of 24 amino acid protein linker.

Based on the above mentioned model configuration (Figure 3-6), it is speculated that both Bph and PYP domains are in close proximity. This in turn brings both chromophore pockets close to each other, through this spatial interface it potentially promotes coupled photoreactions between PYP and Bph domains as observed in UV-Visible measurements under blue light irradiation in the previous chapter. However, just based on dark state structural model of Ppr is inadequate to explain the coupled photoreaction seen under blue light irradiation. Another experiment of SAXS measurements with Ppr subjected to different light conditions aims to further clarify this coupled photoreaction phenomenon.

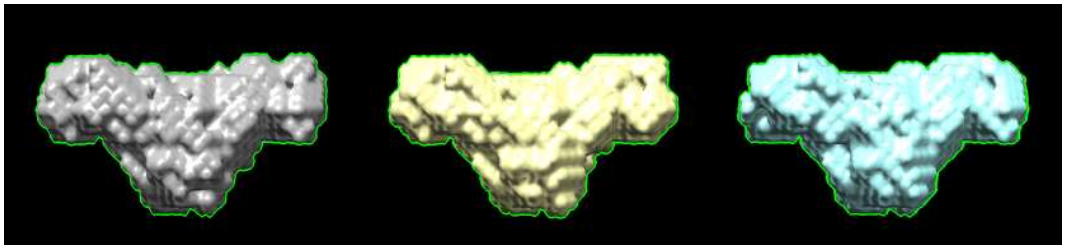

**Front**

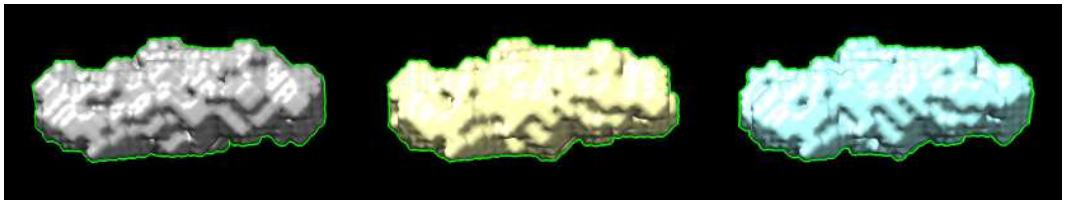

**Side**

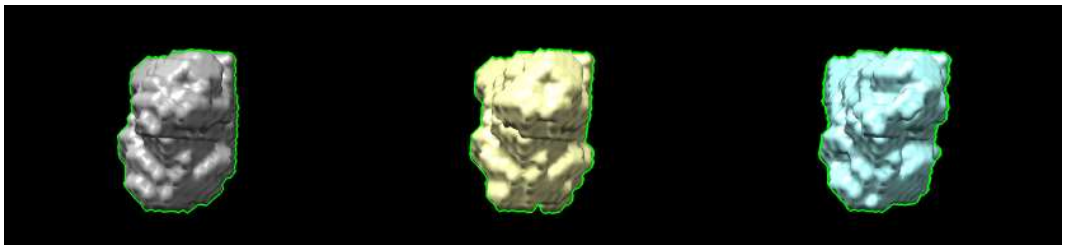

**Top**

**Figure 3-5.** Simulated models of dark state H-H-Ppr based on cluster 7 from Fig. 3-4 as initial guess.

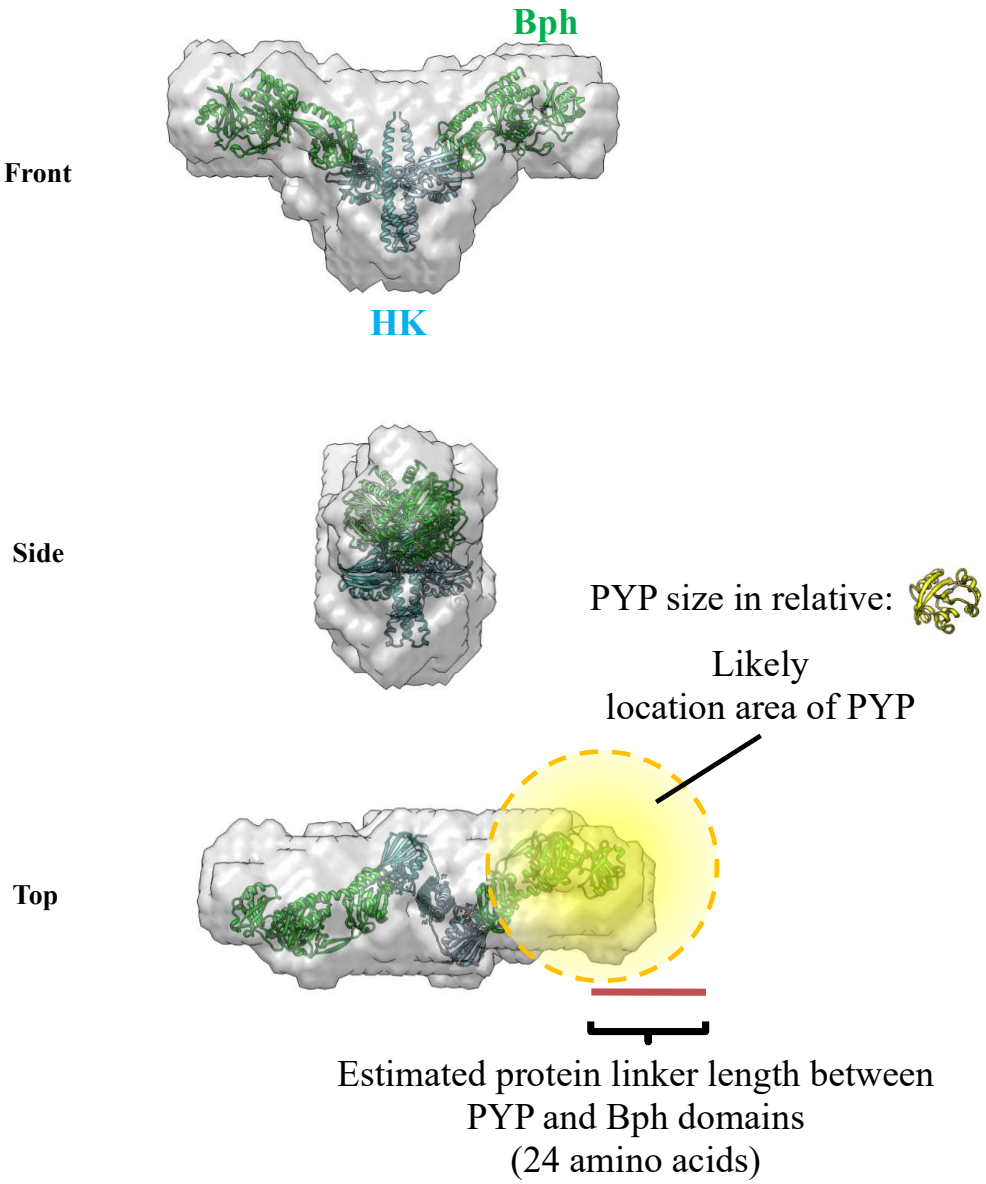


**Figure 3-6.** Manual fitting of X-ray crystallographic data from protein data bank for each domains into *ab initio* modeling envelope. Bph from *Deinococcus radiodurans* (PDB code: 4Q0J) ; HK from *Thermotoga maritama* (PDB code: 2C2A). PYP domain is suspected to be located within the yellow zone.

### 3.3.2 Tertiary structure evaluation of Ppr based on SAXS

In order to investigate the tertiary structure difference between Ppr of different light irradiation states, qualitative information on the "foldedness" of Ppr is accessed through Kratky analysis. SAXS measurement H-A-Ppr and A-H-Ppr were performed in the dark and under red or blue light irradiation. Measured data is represented by Kratky plot as demonstrated in Figure 3-7A and Figure 3-7B. Signal to noise ratio for H-A-Ppr is low due to low sample concentration was used as higher concentration results in sample aggregations. From Kratky analysis of the H-A-Ppr and A-H-Ppr, no tertiary structure difference is observed between their respective dark state and light irradiated states. Together with the observations from Chapter 2, $PYP_L$ from H-A-Ppr and Bph* from A-H-Ppr does not trigger any large tertiary structure change to Ppr.

Comparing between dark state and red light irradiated H-H-Ppr, Kratky plot shows near identical curves (Figure 3-8). Similar to A-H-Ppr under light irradiation, H-H-Ppr under red light irradiation only results in Bph* photoproduct. In short, this signifies no large tertiary structure difference between dark state and red light irradiated H-H-Ppr. However, it should not be ruled out that minor protein structure changes might be present between these irradiation conditions. Changes to the chromophore environment as indicated by UV-Visible measurements may still affect the interactions with neighboring amino acid chains, possibly inducing intradomain changes beyond the resolving power of the current measuring method.

As for H-H-Ppr under blue light irradiation, Kratky plot in Figure 3-9A indicates a substantial difference around $Q = 0.05$ $Å^{-1}$ between dark state H-H-Ppr and blue light irradiated H-H-Ppr. Moreover, when adopting the early and late phase blue light irradiation concept as demonstrated in Chapter 2, it is observed that the difference between dark and blue light irradiated H-H-Ppr is larger in the early phase of blue light irradiation (Figure 3-9B). The

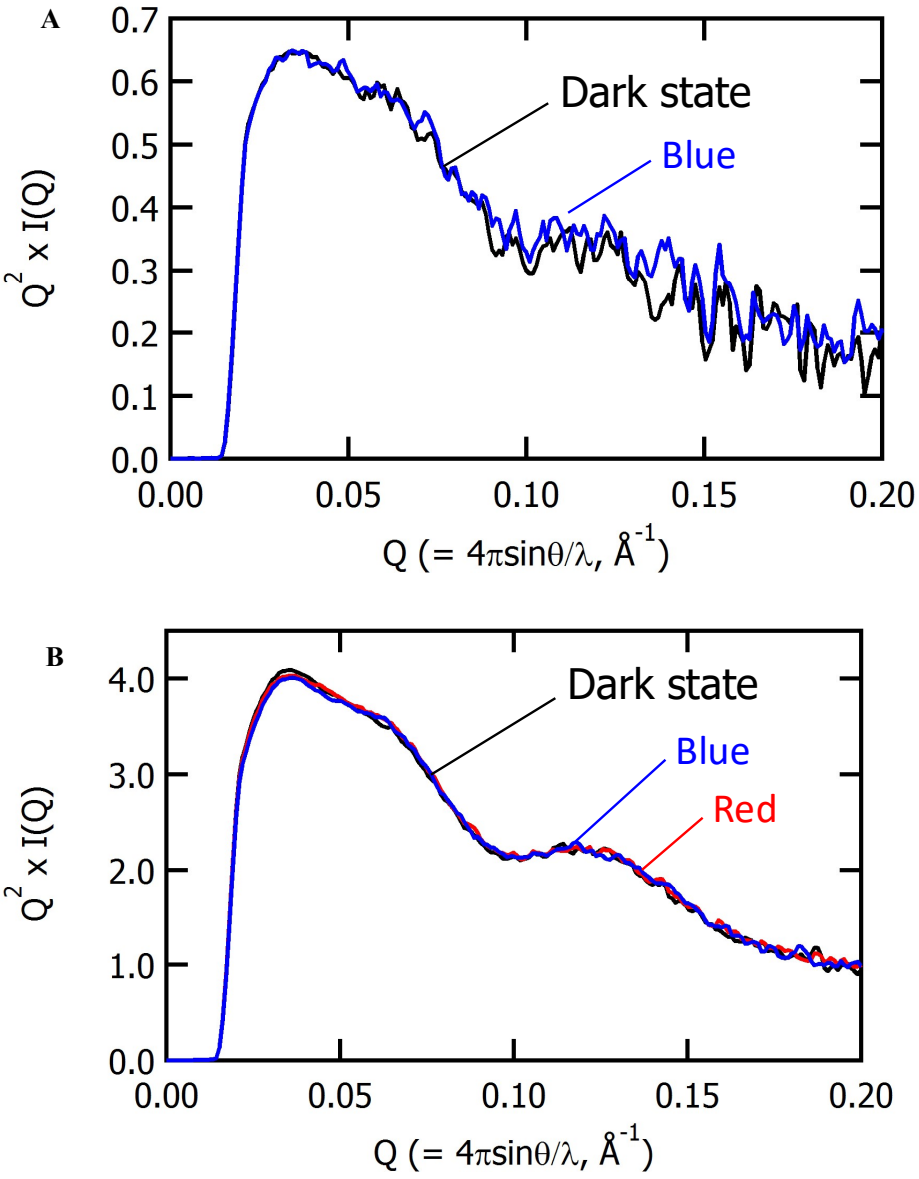


**Figure 3-7.** (A) Kratky plot of dark state Holo-Apo-Ppr (black) and blue light irradiated Holo-Apo-Ppr (blue). (B) Kratky plot of dark state Apo-Holo-Ppr (black), red light irradiated Apo-Holo-Ppr (red) and blue light irradiated Apo-Holo-Ppr (blue).

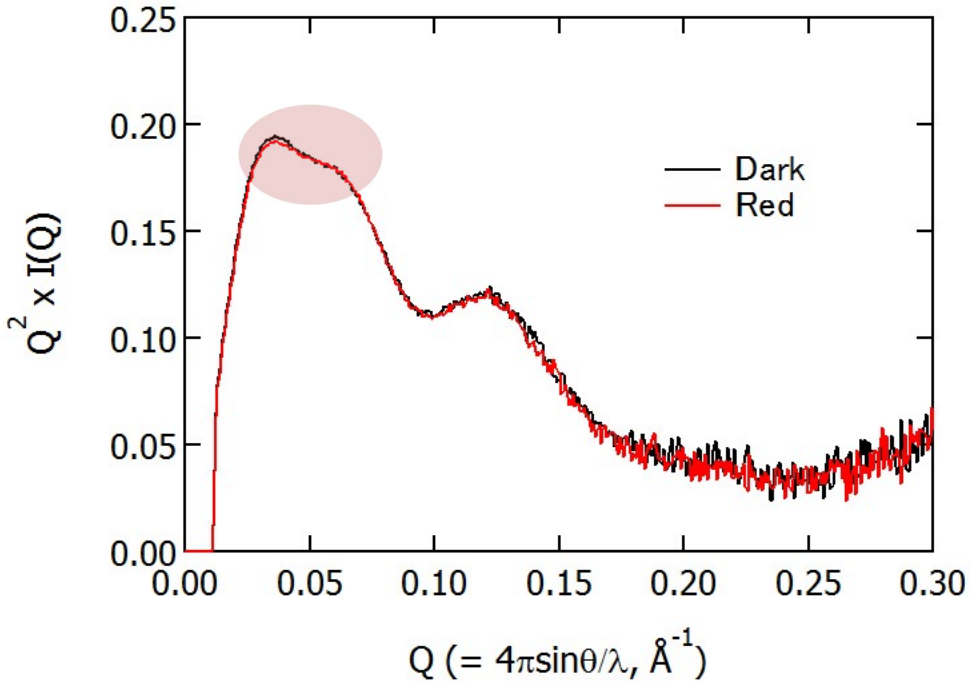


**Figure 3-8.** Kratky plot of dark state Holo-Holo-Ppr (black) and red light irradiated Holo-Holo-Ppr (red).

amount of difference over time is clearly demonstrated in Figure 3-10 where the integrated area difference between $0.025 < Q < 0.07$ at different time is plotted over time scale x-axis. It is clearly shown that the amount of difference increases over time in the early phase of blue light irradiation (initial 250 seconds). In the late phase (beyond 250 seconds), the area of difference partially decrease over time.

Direct observations indicate that blue light irradiation on H-H-Ppr initially causes a large tertiary structure change to Ppr. As Ppr is subjected to longer exposure to blue light, the structure difference is suppressed and possibly return to its original conformation in partial. Together with the information from Chapter 2 concerning the proposed photoreactions under blue light, the increase and decrease of structure difference corresponds to the changes of the coupled photoreactions between $PYP_M$ and Bph. On top of that, the time scale of the changes closely matches with each other, the turning point around 250 seconds of blue light irradiation. This correlation suggests that $PYP_M$ intermediate is an important factor in triggering structural changes seen in Ppr. Though, it is worth noting that the suppressed structure difference at the late phase only suggests structure change suppressed by Bph* formation. It is still unknown the Ppr recovers to which exact structure form, could be towards the original dark state conformation or other intermediate form. Radius of gyration of H-H-Ppr in each light condition remains similar (Table 3-3). This could mean although there is a change in the shape of the protein, the overall size of Ppr is not affected.

One possible structural changes would be the relocation of PYP domain. To demonstrate this, the approximated model from Figure 3-6 is used as the reference to infer and adjust the position of PYP domain. Scattering intensity curves could then be simulated from these rigid models using CRYSOL algorithm (49). The simulated intensity curves plotted as Kratky plots

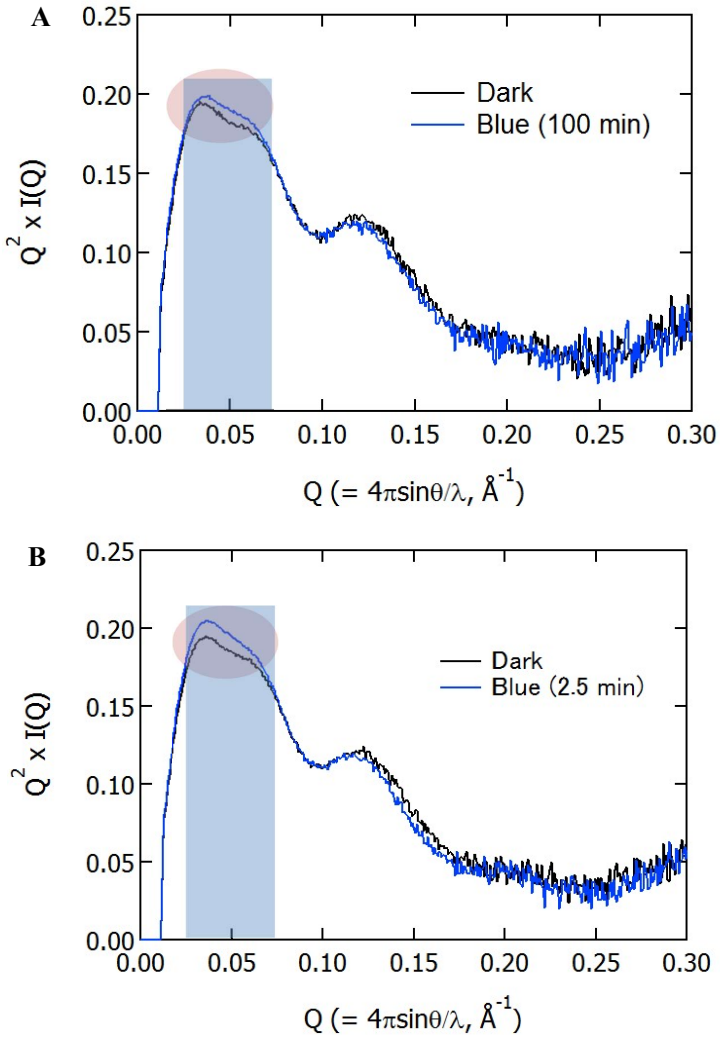


**Figure 3-9.** Kratky plot of dark state Holo-Holo-Ppr (black) and blue light irradiated Holo-Holo-Ppr (red). Panel A compares between dark state and blue light state at 100 minutes. Panel B compares between dark state and blue light state at 2.5 minutes. Circle area indicates the region with substantial difference between dark and light irradiated state. Blue rectangle area indicates the area used for integration calculation in Figure 3-10.

are compared with each other (Figure 3-11). With the PYP domain relocate from outer end towards the inner region next to Bph domain, the difference between two intensity curves demonstrates a homologous difference feature seen between dark state and blue light state of H-H-Ppr in Figure 3-9. Though this is by no means the definite pathway of structural changes adopted by Ppr. This comparison serves as an insight to one of the way to approximate various structure changes when a more definite protein crystallography information for each Ppr domain is available in the future.

In a brief conclusion remark for Chapter 3, H-H-Ppr in solution assumes a dimeric structure. Modeling simulation based on dark state H-H-Ppr demonstrate an open Y shape structure, one monomer on each side. Both monomers are held together by HK domains at the center. Both Bph and PYP domains occupy the outer structure, assumed to be in relative close proximity. This neighboring configuration between PYP and Bph possibly promotes coupling reaction between these two domains. When subjected to blue light irradiation, H-H-Ppr is observed to alter its tertiary structure. This changes is linked to the formation of $PYP_M$ as evident by the increased amount of $PYP_M$ in the initial 250 sec of blue light irradiation in Chapter 2. On the other hand, structure change is suppressed by Bph* accumulation at longer blue light irradiation period. Together with the low-resolution 3D modeling of dark state H-H-Ppr, given the relative close proximity of PYP and Bph domains to each other, isomerization of pCA chromophore in its excited state forming $PYP_M$ would perturbed the PYP domain structure which in turn affects its neighboring Bph domain. Exactly how the two domains changes their structure still subject to further investigation. Current limitation is blue light irradiation of H-H-Ppr produces a mixture of several photospecies at PSS, presenting a challenge of separating these photospecies for modeling simulation.

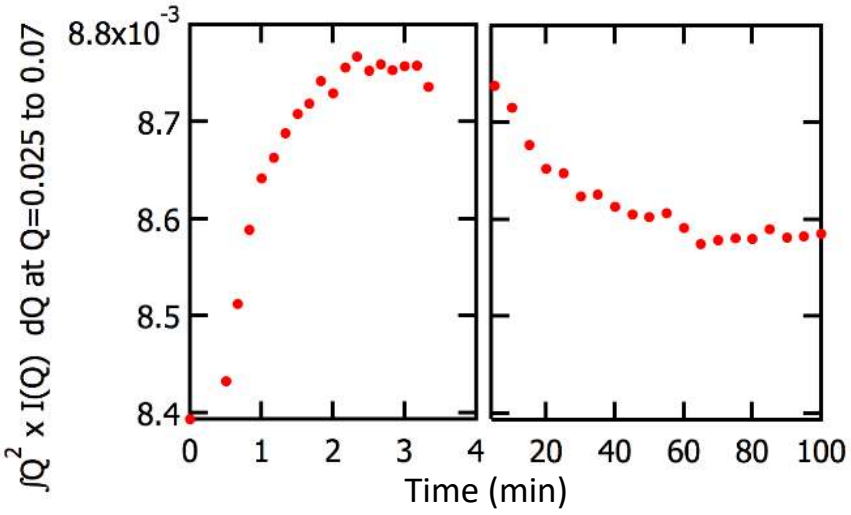


**Figure 3-10.** The area of intensity between $0.025 < Q < 0.07$ of Holo-Holo-Ppr under blue light irradiation.

**Table 3-3.** The radius of gyration and forward scattering intensity of Holo-Holo-Ppr from static SAXS measurement.

| | **Rg (Å)** | **I(0)/conc.** |
|---|---|---|
| **Dark** | 59.7 ± 1.6 | 66.5 ± 1.5 |
| **Red irradiation** | 59.1 ± 1.8 | 65.4 ± 1.6 |
| **Blue irradiation** | 58.7 ± 1.5 | 66.5 ± 1.3 |

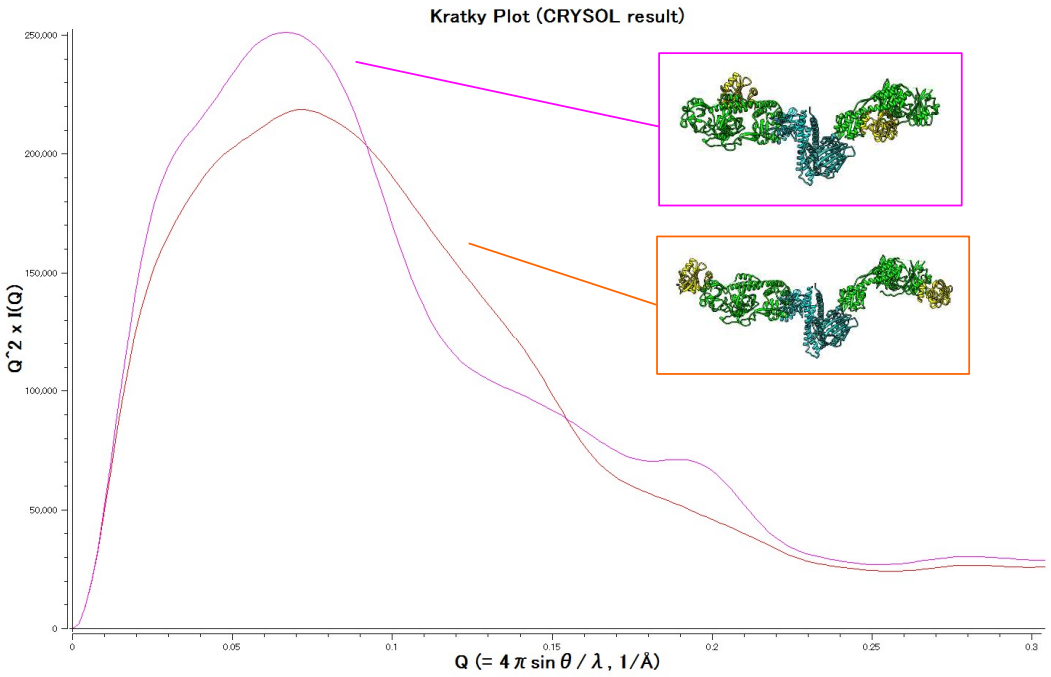


**Figure 3-11.** Scattering intensity simulation in pure water environment via CRYSOL algorithm. (PRIMUS program)

## CHAPTER 4: General Conclusion

The properties of Ppr under different light irradiation has been successfully characterized in this study. Consolidating the observations from both experimental chapters, Ppr can be categorized into structurally silent and active form to explain the reactions involved in different sample and light conditions. Figure 4-1 summarizes the conditions that results in a structurally silent Ppr. H-A-Ppr contains pCA chromophore and absorbs only blue light. H-A-Ppr exposed to blue light irradiation mainly forms $PYP_L$ photoproduct. This light activated H-A-Ppr does not experience any large tertiary structure change. A-H-Ppr contains BV chromophore and absorbs both blue and red light. Under both type of light irradiation separately induce the same Bph* photoproduct. H-H-Ppr contains both pCA and BV chromophore absorbs both blue and red light. Though, red light irradiation only photoconverts Bph domain, resulting in Bph* photoproduct. In both A-H-Ppr and H-H-Ppr where there is only Bph* accumulation, Ppr does not undergoes any large tertiary structure change.

Figure 4-2 summarizes the conditions where Ppr demonstrates tertiary structure change. Ppr structure change occurs in the condition of H-H-Ppr exposed to blue light irradiation. Chapter 2 has described the two time domains of blue light irradiation, early phase for the initial 5 minutes of irradiation, late phase for beyond 5 minutes of irradiation. In the early phase of blue light irradiation, the major photoreaction involves the accumulation of $PYP_M$. Formation of $PYP_M$ is only observed in H-H-Ppr and largely absent in H-A-Ppr. It is probably due to the close proximity of PYP domain to Bph domain, bringing both BV and pCA chromophore close to each other. Through a yet unclear mechanism, presence of BV in H-H-Ppr is thought to promote and stabilize the formation of $PYP_M$. From other studies on *Hh*-PYP, $PYP_M$ is responsible for the partial unfolding of the *Hh*-PYP protein (38). Assuming PYP domain of Ppr undergoes similar unfolding, this would in turn affect the structural conformation of the Bph

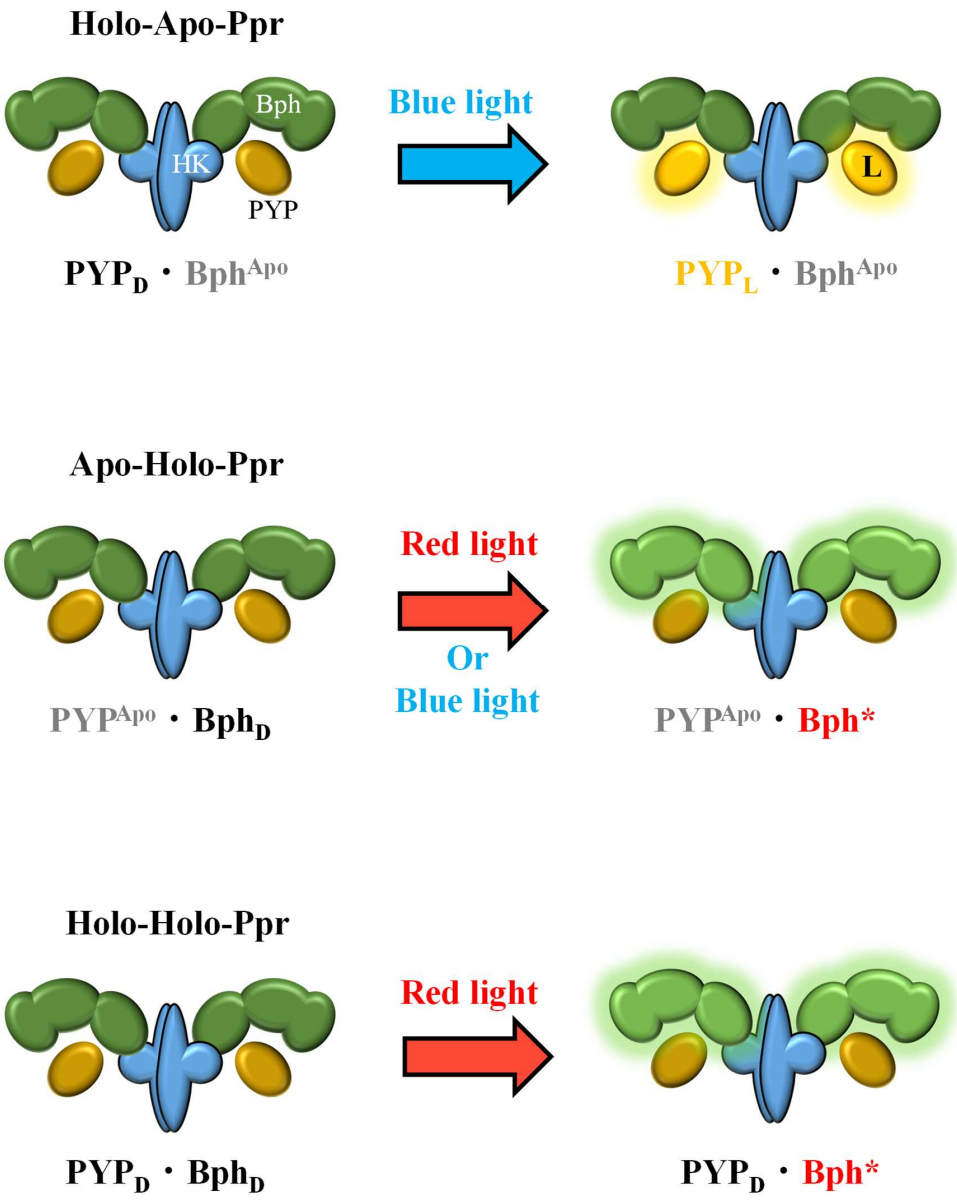


**Figure 4-1.** Reaction scheme of structurally silent Ppr.

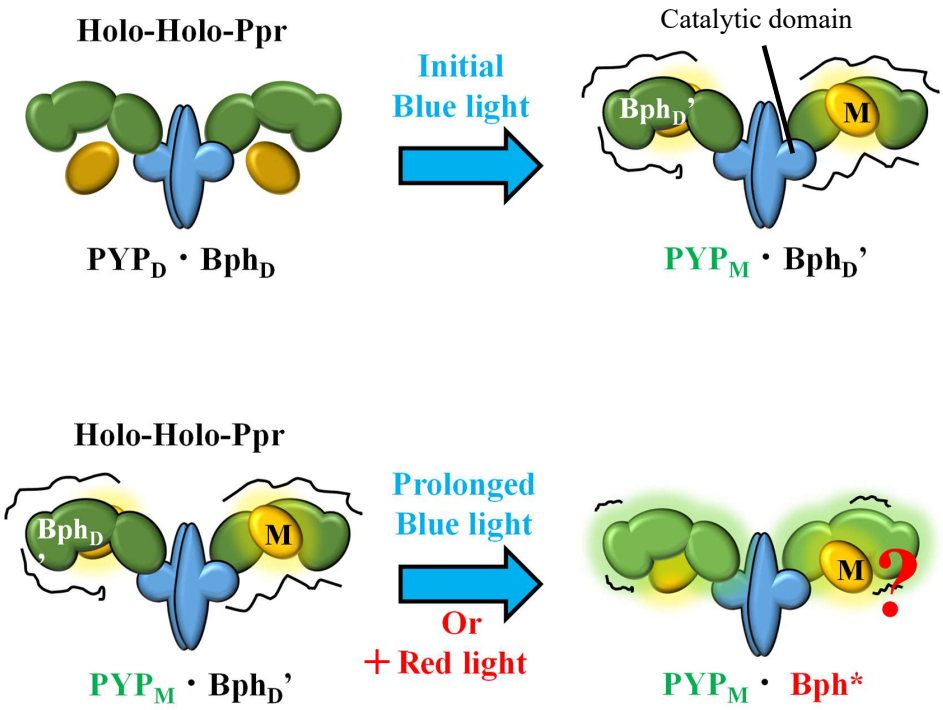


**Figure 4-2.** Reaction scheme of structurally active Ppr.

domain through close proximity interaction. Such changes would explain the UV-Vis absorbance wavelength shift of Bph which indicates the BV chromophore environment being perturbed. In the event that Bph domain is structurally affected, it is compelling to reason that HK domain would also experience some sort of changes. Given that C-terminal end of Bph domain is located close to the catalytic domain of HK, this region will experience the most effect. In HK, catalytic domain is responsible in the phosphorylation activity via adenosine triphosphate (ATP) molecule bound within it. In overall, this study suggests that under blue light irradiation, formation of $PYP_M$ in H-H-Ppr will affect the enzymatic activity of HK domain. However, further study is needed to clarify if the changes is an upregulation or downregulation on HK activity.

As for the late phase time domain of blue light irradiation, UV-Vis measurements in Chapter 2 indicates the photoreaction involves the accumulation of Bph*. Within this time domain, Chapter 3 reveals the structural difference of light state H-H-Ppr compared to dark state is suppressed. The current interpretation points to H-H-Ppr partially recovers to its native conformation. However, instead of recovers to native structure, the possibility of H-H-Ppr takes on an entirely different structural conformation could not be excluded. Nevertheless, HK activity changes triggered by $PYP_M$ would be suppressed when Bph* is accumulated. Considering the point that accumulation of Bph* suppressed the structural changes, other light conditions that promotes formation of Bph* should produce similar result. This includes an addition of red light irradiation or using white light irradiation. Further study is required to elucidate the precise structural difference between $PYP_M \cdot Bph_D$' and $PYP_M \cdot$ Bph*.

Considering Ppr protein is found in *R. centenum*, a motile photosynthetic bacterium, it is conceivable that this protein could be part of the regulation pathway that controls the

movement of bacterium depending on light environment. Findings from Kreutel indicate the truncated histidine kinase domain of Ppr has a functional role in CheW binding, in which CheW is a type of protein that helps regulate chemotaxis (23). One of the way to examine for the involvement of Ppr in biological function is to analyze its kinase activity. So far, there are two studies that directly report the kinase activity of Ppr (20, 37). Jiang reports on the PYP domain seems to suppress the kinase activity by comparing the difference between Apo-Apo-Ppr and Holo-Apo-Ppr, with kinase activity in Holo-Apo-Ppr further suppressed under light condition. On the other hand, Kyndt's group shown the kinase activity of Ppr, while minimal in dark state, is increased in the presence of red light. Considering both separate observations, it is possible photoactivated Bph domain upregulates kinase activity while photoactivated PYP domain downregulates kinase activity. However, our SAXS measurements only indicates largest structural change of H-H-Ppr under the blue light in the initial 250 sec duration, which corresponds to photoactivation of PYP domain. Other light conditions and Ppr variants shown no similar or any variants of large structural difference from SAXS measurements that could suggests any relation to kinase regulation through structural change of Ppr. This dissimilarity could be due to different experimental condition used in different studies or there could be yet more mechanisms involved in Ppr remain undiscovered. This renders the functional active form of Ppr remains unclear until a comparable experimental condition is carried out to clarify it. Though one could ascertain that PYP domain plays a role together with Bph domain as a biological On/Off photoswitch, potentially sensing different light qualities to regulate downstream chemical reactions.

From a living cell perspective, it should be expensive in energy to maintain a two light sensing system over the simpler one light sensing system. There should be certain advantages offered by a dual-light sensing system to justify the use of additional resource. Otherwise, biological evolution process would have phase out this system if not useful for survival. Seeing

as *R.centenum* lives in a water environment and depends on sunlight for photosynthesis, it could be thought that Ppr functions to detect the ratio of beneficial red light and harmful blue light (avoiding UV damage). As water medium absorbs more strongly on red light, the photosynthetic bacteria has to stay near the surface for photosynthesis, at the same time avoid overexposure to harmful blue light. Utilizing only one light sensing system might not result in optimal placement. Only sensing blue light, bacteria would move too deep into the depth of water. With only red light sensor, it might risk overexposure to UV light. With a dual-light sensor, this allows the bacteria to locate a moderate water depth for optimal chance of survival.

**Acknowledgement**

This dissertation has been accomplished with the support from various people and I would like to express my gratitude for their valuable assistance.

First and foremost, I would like to sincerely give my heartfelt thanks to my core supervisor Professor Hironari Kamikubo for his guidance and advises throughout the whole study, not just assisting in the research project but also sharing his experiences and knowledge regarding the life and conducts of a research scientist. I also appreciates the comments and advices provided by Professor Michiya Fujiki, Visiting Professor Takahiro Honda and Associate Professor Takashi Matsuo. I am grateful to Assistant Professor Yoichi Yamazaki for his in depth advice and discussion on Ppr protein and spectroscopy analyses, and also to Assistant Professor Yugo Hayashi for his input and experience regarding SAXS techniques and analysis.

To all my fellow lab members and colleagues, thank you for showing me around places and for those candid discussions about research in general. Also, directing my thanks to NAIST for the facilities provided and a team of wonderful dedicated staffs making sure my study here was as smooth as possible.

In addition, I am thankful to the Japanese government (Ministry of Education, Culture, Sports, Science and Technology) for the financial support during my stay in Japan and also to the Japanese community in general for the wonderful experience given to me as an international student.

Last but not least, I would like to express my appreciation to my family for their love and support, especially for their understanding of my desire to further pursue knowledge far from home for an extended time.

**References**


1. Fankhauser, C. 2001. The phytochromes, a family of red/far-red absorbing photoreceptors. J. Biol. Chem. 276: 11453–11456.

2. Montgomery, B.L., and J.C. Lagarias. 2002. Phytochrome ancestry: sensors of bilins and light. Trends Plant Sci. 7: 357–366.

3. Rockwell, N.C., Y.-S. Su, and J.C. Lagarias. 2006. Phytochrome structure and signaling mechanisms. Annu. Rev. Plant Biol. 57: 837–858.

4. Davis, S.J., A.V. Vener, and R.D. Vierstra. 1999. Bacteriophytochromes: phytochrome-like photoreceptors from nonphotosynthetic eubacteria. Science. 286: 2517–2520.

5. Giraud, E., and A. Verméglio. 2008. Bacteriophytochromes in anoxygenic photosynthetic bacteria. Photosynth. Res. 97: 141–153.

6. Auldridge, M.E., and K.T. Forest. 2011. Bacterial phytochromes: more than meets the light. Crit. Rev. Biochem. Mol. Biol. 46: 67–88.

7. Bhoo, S.-H., S.J. Davis, J. Walker, B. Karniol, and R.D. Vierstra. 2001. Bacteriophytochromes are photochromic histidine kinases using a biliverdin chromophore. Nature. 414: 776–779.

8. Wagner, J.R., J.S. Brunzelle, K.T. Forest, and R.D. Vierstra. 2005. A light-sensing knot revealed by the structure of the chromophore-binding domain of phytochrome. Nature. 438: 325–331.

9. Giraud, E., J. Fardoux, N. Fourrier, L. Hannibal, B. Genty, P. Bouyer, B. Dreyfus, and A. Verméglio. 2002. Bacteriophytochrome controls photosystem synthesis in anoxygenic bacteria. Nature. 417: 202–205.

10. Rottwinkel, G., I. Oberpichler, and T. Lamparter. 2010. Bathy phytochromes in rhizobial soil bacteria. J. Bacteriol. 192: 5124–5133.

11. Giraud, E., S. Zappa, L. Vuillet, J.-M. Adriano, L. Hannibal, J. Fardoux, C. Berthomieu, P. Bouyer, D. Pignol, and A. Verméglio. 2005. A new type of bacteriophytochrome acts in tandem with a classical bacteriophytochrome to control the antennae synthesis in Rhodopseudomonas palustris. J. Biol. Chem. 280: 32389–32397.

12. Jaubert, M., J. Lavergne, J. Fardoux, L. Hannibal, L. Vuillet, J.-M. Adriano, P. Bouyer, D. Pignol, E. Giraud, and A. Verméglio. 2007. A singular bacteriophytochrome acquired by lateral gene transfer. J. Biol. Chem. 282: 7320–7328.

13. Favinger, J., R. Stadtwald, and H. Gest. 1994. Rhodospirillum centenum sp. nov. Validation of the publication of new names and new combinations previously effectively published outside the IJSB, List.

14. Favinger, J., R. Stadtwald, and H. Gest. 1989. Rhodospirillum centenum, sp. nov., a thermotolerant cyst-forming anoxygenic photosynthetic bacterium. Antonie van Leeuwenhoek. 55: 291–296.

15. Kawasaki, H., Y. Hoshino, H. Kuraishi, and K. Yamasato. 1992. Rhodocista centenaria gen. nov., sp. nov., a cyst-forming anoxygenic photosynthetic bacterium and its phylogenetic position in the Proteobacteria alpha group. J. Gen. Appl. Microbiol. 38: 541–551.

16. Ragatz, L., Z.-Y. Jiang, C.E. Bauer, and H. Gest. 1995. Macroscopic phototactic behavior of the purple photosynthetic bacterium Rhodospirillum centenum. Arch. Microbiol. 163: 1–6.

17. Ragatz, L., Z.-Y. Jiang, C. Bauer, and H. Gest. 1994. Phototactic purple bacteria. Nature. 370: 104.

18. Jiang, Z.-Y., H. Gest, and C.E. Bauer. 1997. Chemosensory and photosensory perception in purple photosynthetic bacteria utilize common signal transduction components. J. Bacteriol. 179: 5720–5727.

19. Jiang, Z.-Y., B.G. Rushing, Y. Bai, H. Gest, and C.E. Bauer. 1998. Isolation of Rhodospirillum centenumMutants Defective in Phototactic Colony Motility by Transposon Mutagenesis. J. Bacteriol. 180: 1248–1255.

20. Jiang, Z., L.R. Swem, B.G. Rushing, S. Devanathan, G. Tollin, and C.E. Bauer. 1999. Bacterial photoreceptor with similarity to photoactive yellow protein and plant phytochromes. Science. 285: 406–409.

21. Lu, Y.-K., J. Marden, M. Han, W.D. Swingley, S.D. Mastrian, S.R. Chowdhury, J. Hao, T. Helmy, S. Kim, and A.A. Kurdoglu. 2010. Metabolic flexibility revealed in the genome of the cyst-forming α-1 proteobacterium Rhodospirillum centenum. BMC Genomics. 11: 325.

22. Berleman, J.E., B.M. Hasselbring, and C.E. Bauer. 2004. Hypercyst mutants in Rhodospirillum centenum identify regulatory loci involved in cyst cell differentiation. J. Bacteriol. 186: 5834–5841.

23. Kreutel, S., A. Kuhn, and D. Kiefer. 2010. The photosensor protein Ppr of Rhodocista centenaria is linked to the chemotaxis signalling pathway. BMC Microbiol. 10: 281.

24. Kyndt, J.A., J.C. Fitch, T.E. Meyer, and M.A. Cusanovich. 2007. The photoactivated PYP domain of Rhodospirillum centenum Ppr accelerates the recovery of the bacteriophytochrome domain after white light illumination. Biochemistry. 46: 8256–8262.

25. Takala, H., A. Björling, O. Berntsson, H. Lehtivuori, S. Niebling, M. Hoernke, I. Kosheleva, R. Henning, A. Menzel, and J.A. Ihalainen. 2014. Signal amplification and transduction in phytochrome photosensors. Nature. 509: 245–248.

26. Burgie, E.S., J. Zhang, and R.D. Vierstra. 2016. Crystal structure of Deinococcus phytochrome in the photoactivated state reveals a cascade of structural rearrangements during photoconversion. Structure. 24: 448–457.

27. Meyer, T.E. 1985. Isolation and characterization of soluble cytochromes, ferredoxins and other chromophoric proteins from the halophilic phototrophic bacterium Ectothiorhodospira halophila. Biochim. Biophys. Acta. 806: 175–183.

28. Meyer, T.E., E. Yakali, M.A. Cusanovich, and G. Tollin. 1987. Properties of a water-soluble, yellow protein isolated from a halophilic phototrophic bacterium that has photochemical activity analogous to sensory rhodopsin. Biochemistry. 26: 418–423.

29. Hoff, W.D., I.H. Van Stokkum, H.J. Van Ramesdonk, M.E. Van Brederode, A.M. Brouwer, J.C. Fitch, T.E. Meyer, R. Van Grondelle, and K.J. Hellingwerf. 1994. Measurement and global analysis of the absorbance changes in the photocycle of the photoactive yellow protein from Ectothiorhodospira halophila. Biophys. J. 67: 1691–1705.

30. Imamoto, Y., M. Kataoka, and F. Tokunaga. 1996. Photoreaction cycle of photoactive yellow protein from Ectothiorhodospira halophila studied by low-temperature spectroscopy. Biochemistry. 35: 14047–14053.

31. Imamoto, Y., M. Harigai, and M. Kataoka. 2004. Direct observation of the pH-dependent equilibrium between L-like and M intermediates of photoactive yellow protein. FEBS Lett. 577: 75–80.

32. Kyndt, J.A., T.E. Meyer, and M.A. Cusanovich. 2004. Photoactive yellow protein, bacteriophytochrome, and sensory rhodopsin in purple phototrophic bacteria. Photochem. Photobiol. Sci. 3: 519–530.

33. Burgie, E.S., T. Wang, A.N. Bussell, J.M. Walker, H. Li, and R.D. Vierstra. 2014. Crystallographic and electron microscopic analyses of a bacterial phytochrome reveal local and global rearrangements during photoconversion. J. Biol. Chem. 289: 24573–24587.

34. Evans, K., A.P. Fordham-Skelton, H. Mistry, C.D. Reynolds, A.M. Lawless, and M.Z. Papiz. 2005. A bacteriophytochrome regulates the synthesis of LH4 complexesin Rhodopseudomonas palustris. Photosynth. Res. 85: 169–180.

35. Evans, K., J.G. Grossmann, A.P. Fordham-Skelton, and M.Z. Papiz. 2006. Small-angle X-ray scattering reveals the solution structure of a bacteriophytochrome in the catalytically active Pr state. J. Mol. Biol. 364: 655–666.

36. Takala, H., A. Björling, M. Linna, S. Westenhoff, and J.A. Ihalainen. 2015. Light-induced changes in the dimerization interface of bacteriophytochromes. J. Biol. Chem. 290: 16383–16392.

37. Kyndt, J.A., J.C. Fitch, S. Seibeck, B. Borucki, M.P. Heyn, T.E. Meyer, and M.A. Cusanovich. 2010. Regulation of the Ppr histidine kinase by light-induced interactions between its photoactive yellow protein and bacteriophytochrome domains. Biochemistry. 49: 1744–1754.

38. Imamoto, Y., and M. Kataoka. 2007. Structure and photoreaction of photoactive yellow protein, a structural prototype of the PAS domain superfamily. Photochem. Photobiol. 83: 40–49.

39. Björling, A., O. Berntsson, H. Takala, K.D. Gallagher, H. Patel, E. Gustavsson, R. St. Peter, P. Duong, A. Nugent, and F. Zhang. 2015. Ubiquitous structural signaling in bacterial phytochromes. J. Phys. Chem. Lett. 6: 3379–3383.

40. Kamikubo, H., T. Koyama, M. Hayashi, K. Shirai, Y. Yamazaki, Y. Imamoto, and M. Kataoka. 2008. The Photoreaction of the Photoactive Yellow Protein Domain in the Light Sensor Histidine Kinase Ppr is Influenced by the C-terminal Domains. Photochem. Photobiol. 84: 895–902.

41. Imamoto, Y., M. Kataoka, and R.S. Liu. 2002. Mechanistic Pathways for the Photoisomerization Reaction of the Anchored, Tethered Chromophore of the Photoactive Yellow Protein and its Mutants¶. Photochem. Photobiol. 76: 584–589.

42. Jacques, D.A., and J. Trewhella. 2010. Small-angle scattering for structural biology—Expanding the frontier while avoiding the pitfalls. Protein Sci. 19: 642–657.

43. Pauw, B.R. 2013. Everything SAXS: small-angle scattering pattern collection and correction. J. Phys. Condens. Matter. 25: 383201.

44. Genick, U.K., G.E. Borgstahl, K. Ng, Z. Ren, C. Pradervand, P.M. Burke, V. Šrajer, T.-Y. Teng, W. Schildkamp, and D.E. McRee. 1997. Structure of a protein photocycle intermediate by millisecond time-resolved crystallography. Science. 275: 1471–1475.

45. Marina, A., C.D. Waldburger, and W.A. Hendrickson. 2005. Structure of the entire cytoplasmic portion of a sensor histidine-kinase protein. EMBO J. 24: 4247–4259.

46. Svergun, D.I. 1999. Restoring low resolution structure of biological macromolecules from solution scattering using simulated annealing. Biophys. J. 76: 2879–2886.

47. Petoukhov, M.V., D. Franke, A.V. Shkumatov, G. Tria, A.G. Kikhney, M. Gajda, C. Gorba,

H.D. Mertens, P.V. Konarev, and D.I. Svergun. 2012. New developments in the ATSAS program package for small-angle scattering data analysis. J. Appl. Crystallogr. 45: 342–350.

48. Volkov, V.V., and D.I. Svergun. 2003. Uniqueness of ab initio shape determination in small-angle scattering. J. Appl. Crystallogr. 36: 860–864.

49. Svergun, D., C. Barberato, and M.H. Koch. 1995. CRYSOL–a program to evaluate X-ray solution scattering of biological macromolecules from atomic coordinates. J. Appl. Crystallogr. 28: 768–773.

**Appendix**

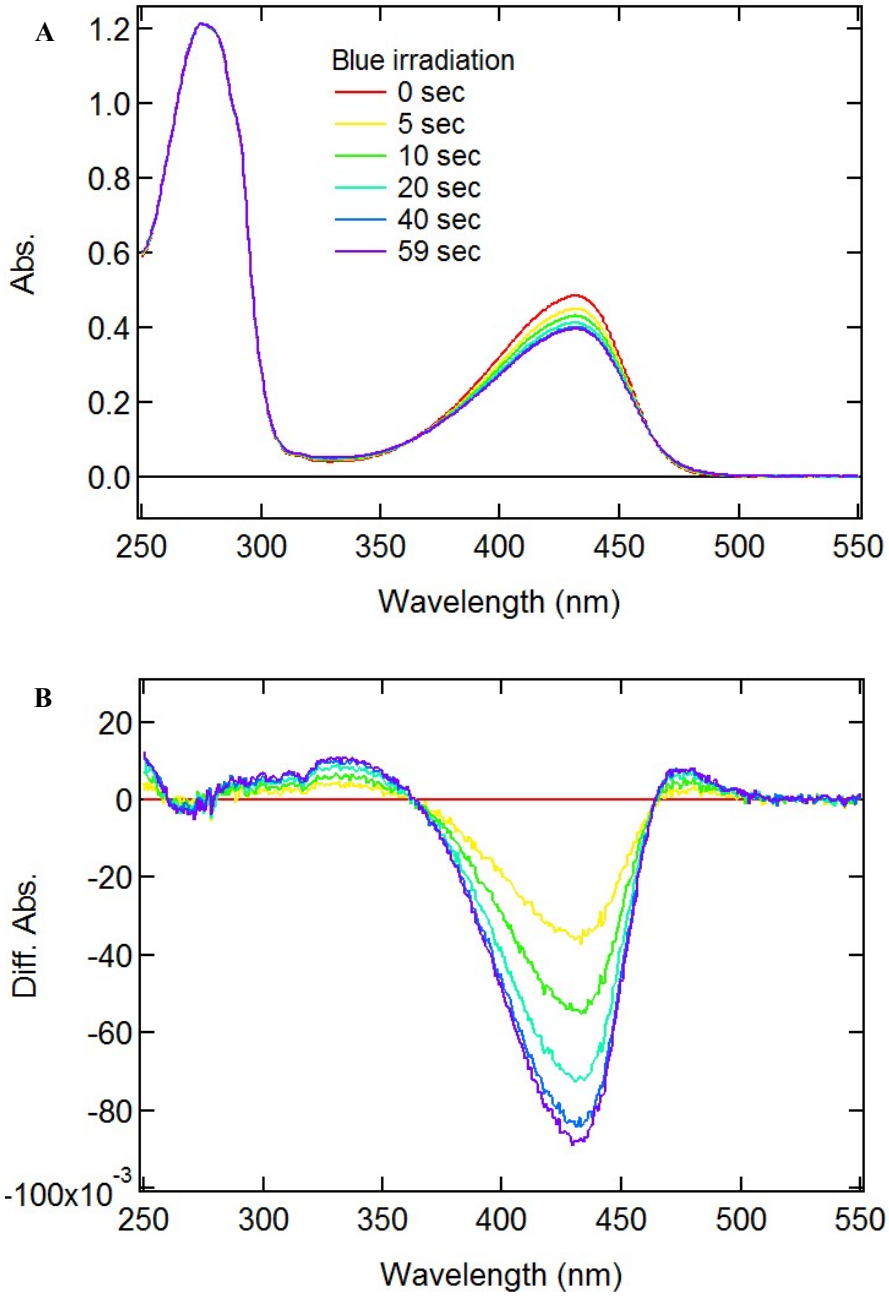


**Figure S1.** (A) Absorption spectra of Holo-Apo-Ppr under blue light irradiation. (B) Blue/dark difference absorption spectra of Holo-Apo-Ppr.

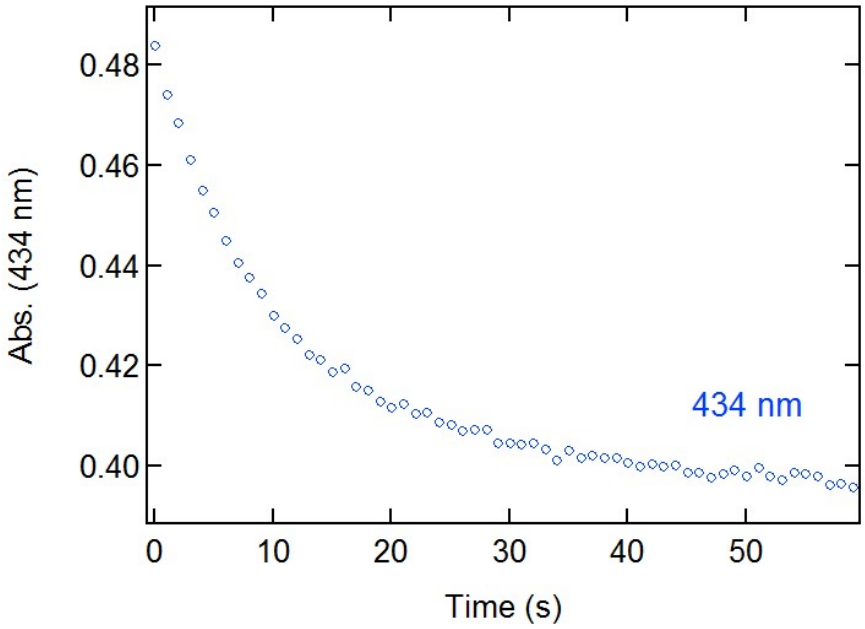


**Figure S2.** Time-resolved absorbance of Holo-Apo-Ppr under red light irradiation at selected wavelength 434 nm at every 1 second interval.

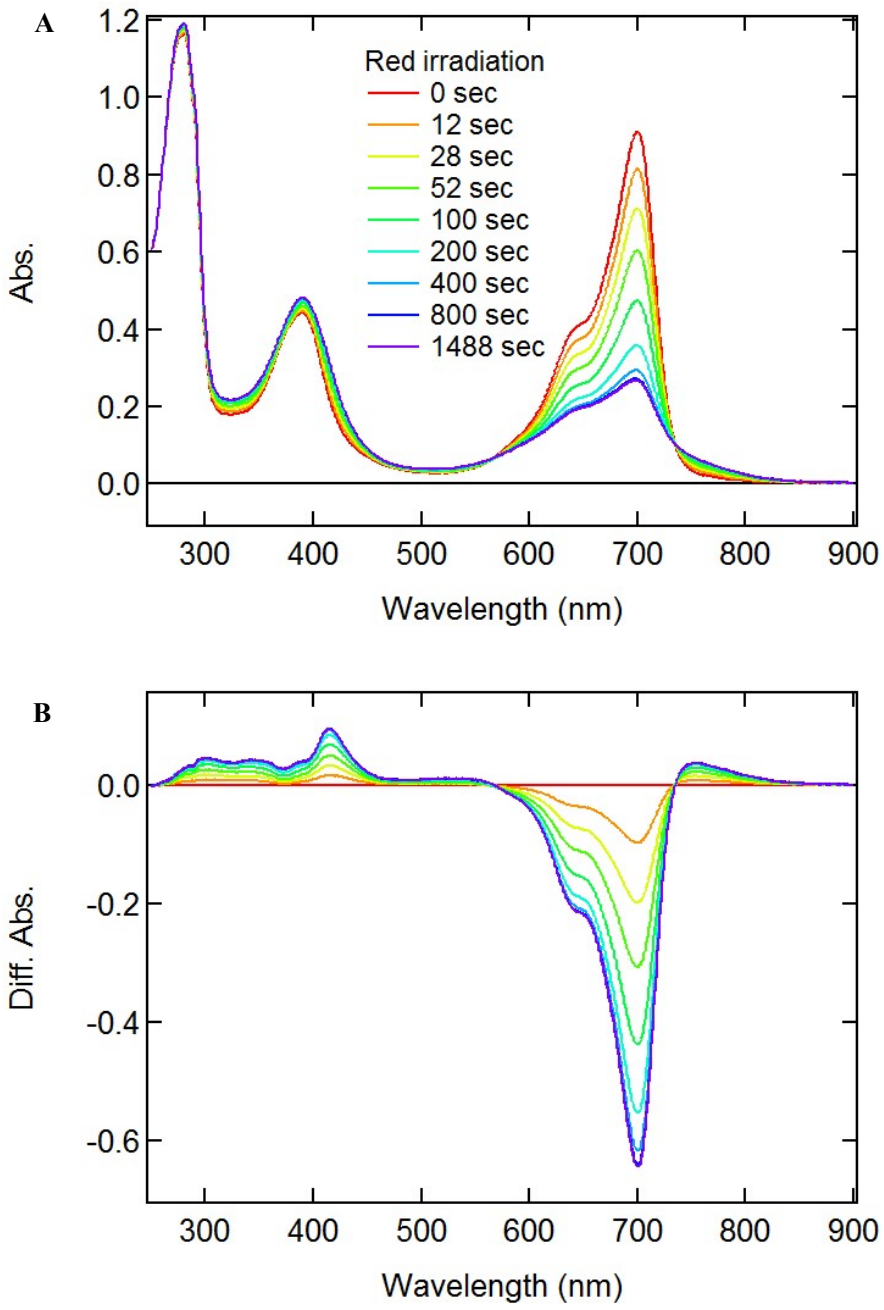


**Figure S3.** (A) Absorption spectra of Apo-Holo-Ppr under red light irradiation. (B) Red/dark difference absorption spectra of Apo-Holo-Ppr.

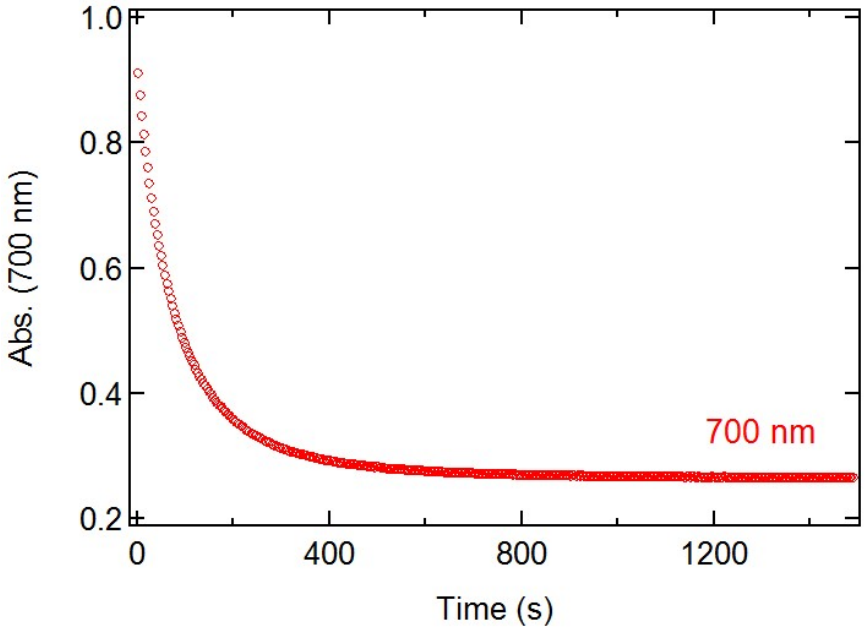


**Figure S4.** Time-resolved absorbance of Apo-Holo-Ppr under red light irradiation at selected wavelength 700 nm at every 4 seconds interval.